

Analysis of the VENUS-3 Experiments

Prepared by R. E. Maerker

Oak Ridge National Laboratory

Prepared for
U.S. Nuclear Regulatory
Commission

AVAILABILITY NOTICE

Availability of Reference Materials Cited in NRC Publications

Most documents cited in NRC publications will be available from one of the following sources:

1. The NRC Public Document Room, 2120 L Street, NW, Lower Level, Washington, DC 20555
2. The Superintendent of Documents, U.S. Government Printing Office, P.O. Box 37082, Washington, DC 20013-7082
3. The National Technical Information Service, Springfield, VA 22161

Although the listing that follows represents the majority of documents cited in NRC publications, it is not intended to be exhaustive.

Referenced documents available for inspection and copying for a fee from the NRC Public Document Room include NRC correspondence and internal NRC memoranda; NRC Office of Inspection and Enforcement bulletins, circulars, information notices, inspection and investigation notices; Licensee Event Reports; vendor reports and correspondence; Commission papers; and applicant and licensee documents and correspondence.

The following documents in the NUREG series are available for purchase from the GPO Sales Program: formal NRC staff and contractor reports, NRC sponsored conference proceedings, and NRC booklets and brochures. Also available are Regulatory Guides, NRC regulations in the *Code of Federal Regulations*, and *Nuclear Regulatory Commission Issuances*.

Documents available from the National Technical Information Service include NUREG series reports and technical reports prepared by other federal agencies and reports prepared by the Atomic Energy Commission, forerunner agency to the Nuclear Regulatory Commission.

Documents available from public and special technical libraries include all open literature items, such as books, journal and periodical articles, and transactions. *Federal Register* notices, federal and state legislation, and congressional reports can usually be obtained from these libraries.

Documents such as theses, dissertations, foreign reports and translations, and non-NRC conference proceedings are available for purchase from the organization sponsoring the publication cited.

Single copies of NRC draft reports are available free, to the extent of supply, upon written request to the Office of Information Resources Management, Distribution Section, U.S. Nuclear Regulatory Commission, Washington, DC 20555.

Copies of industry codes and standards used in a substantive manner in the NRC regulatory process are maintained at the NRC Library, 7920 Norfolk Avenue, Bethesda, Maryland, and are available there for reference use by the public. Codes and standards are usually copyrighted and may be purchased from the originating organization or, if they are American National Standards, from the American National Standards Institute, 1430 Broadway, New York, NY 10018.

DISCLAIMER NOTICE

This report was prepared as an account of work sponsored by an agency of the United States Government. Neither the United States Government nor any agency thereof, or any of their employees, makes any warranty, expressed or implied, or assumes any legal liability of responsibility for any third party's use, or the results of such use, of any information, apparatus, product or process disclosed in this report, or represents that its use by such third party would not infringe privately owned rights.

Analysis of the VENUS-3 Experiments

Manuscript Completed: January 1989
Date Published: August 1989

Prepared by
R. E. Maerker

Oak Ridge National Laboratory
Operated by Martin Marietta Energy Systems, Inc.

Oak Ridge National Laboratory
Oak Ridge, TN 37831

Prepared for
Division of Engineering
Office of Nuclear Regulatory Research
U.S. Nuclear Regulatory Commission
Washington, DC 20555
NRC FIN B0415
Under Contract No. DE-AC05-84OR21400

ABSTRACT

The results of applying a hybrid superposition-synthesis calculational method to a mockup of a three-dimensional geometry involving a partial length shield assembly (PLSA) at the VENUS-3 facility in Mol, Belgium, are described. Comparisons of transport calculations using the method and many measurements involving nickel, indium, and aluminum dosimeters indicate agreement generally to within five percent if effects of inaccuracies in the dosimeter cross sections are minimized and proper orientation of the coordinate system used in the synthesis procedure is observed. These conclusions bode well for the success of this method in solving neutron transport problems involving the use of PLSAs in light water reactors to reduce core leakage in pressurized thermal shock programs.

A second report describing the experimental details of the measurements will serve as companion documentation to this one and will be furnished by the Studiecentrum voor Kernenergie/Centre d'Etude de l'Energie Nucléaire, Mol, Belgium.

TABLE OF CONTENTS

	<u>Page</u>
FIGURE LIST	vii
TABLE LIST	ix
ACKNOWLEDGMENTS	xi
EXECUTIVE SUMMARY	xiii
1. INTRODUCTION AND BACKGROUND	1
2. THE VENUS-3 FACILITY AND AVAILABLE MEASURED RESULTS	3
2.1 GENERAL	3
2.2 GEOMETRY	3
2.3 SOURCE DESCRIPTION	7
2.4 ABSOLUTE SOURCE NORMALIZATION	9
2.5 RESULTS OF THE EQUIVALENT FISSION FLUX MEASUREMENTS	9
3. DESCRIPTION OF THE CALCULATIONS	17
3.1 FLUX SUPERPOSITION-SYNTHESIS MODEL	17
3.2 MODELING OF THE VENUS-3 GEOMETRY	20
3.3 SOME DETAILS OF THE CALCULATIONS	22
3.4 RESULTS OF THE CALCULATIONS	23
4. COMPARISON OF THE MEASUREMENTS AND CALCULATIONS	42
5. DISCUSSION AND CONCLUSIONS	54
6. REFERENCES	57
APPENDIX	A-1

FIGURE LIST

	<u>Page</u>
1. Plan view of the VENUS-3 facility showing the location of the nickel dosimeters used in the early run of March 1988, and the coordinate system defined by SCK/CEN	5
2. Elevation view of the VENUS-3 facility showing the substitution of stainless steel rods for oxide fuel in the lower halves of five peripheral pins	6
3. Illustrating the region where the flux superposition-synthesis procedure may break down if the relative transmissions of the upper and lower peripheral core media are significantly different	19
4. Plan view of the VENUS-3 facility as defined using the variable mesh option with X-Y geometry in DOT-4	21

TABLE LIST

	<u>Page</u>
1. Comparison of source profiles at corresponding locations in the PLSA and unmodified regions	8
2. Measured nickel equivalent fission fluxes at 100% power at all locations except the core barrel	10
3. Measured nickel equivalent fission fluxes at 100% power at the core barrel locations	11
4. Locations and results for measured supplemental nickel equivalent fission fluxes at 100% power	13
5. Locations and results for measured indium equivalent fission fluxes at 100% power	14
6. Locations and results for measured aluminum equivalent fission fluxes at 100% power	15
7. Remaining dosimeters and their locations	16
8. Neutron transmission through UO ₂ relative to stainless steel in the VENUS-3 PLSA geometry	19
9. Values of some discrete ordinates parameters input to DOT 4 and ANISN	23
10. Calculated nickel reaction rate components at locations in the inner baffle and PLSA	24
11. Calculated nickel reaction rate components at locations in the outer baffle	25
12. Calculated nickel reaction rate components at locations in the core barrel	26
13. Calculated nickel reaction rate components for the supplementary locations	31
14. Calculated indium reaction rate components for all locations	35
15. Calculated aluminum reaction rate components	40

TABLE LIST
(Continued)

	Page
16. Absolute comparisons of the nickel reaction rates in the inner baffle and PLSA in units of reactions per second per nucleus at 100% power (early run)	43
17. Absolute comparisons of the nickel reaction rates in the outer baffle in units of reactions per second per nucleus at 100% power (early run)	44
18. Absolute comparisons of the nickel reaction rates in the core barrel in units of reactions per second per nucleus at 100% power (early run)	45
19. Absolute comparisons of the nickel reaction rates in units of reactions per second per nucleus at 100% power (supplementary run)	48
20. Absolute comparisons of the indium reaction rates in units of reactions per second per nucleus at 100% power	50
21. Absolute comparisons of the aluminum reaction rates in units of reactions per second per nucleus at 100% power	53
22. Comparison between measured and calculated ^{235}U and ^{252}Cf fission spectrum averaged cross sections for nickel, indium, and aluminum	54
A.1. Calculated neptunium reaction rate components and resulting equivalent fluxes	A-3

ACKNOWLEDGMENTS

This analysis was heavily dependent on the cooperation of several people at the Studiecentrum voor Kernenergie/Centre d'Etude de l'Energie Nucléaire for providing information on the VENUS-3 facility and the results of many measurements conducted in it. In particular, Leon Leenders supplied drawings and dimensions that more than adequately described the details of the VENUS-3 geometry, and in addition obtained and transmitted the excellent relative source data, so necessary for the analysis, in a timely fashion despite the presence of some disruptions caused by a transition period in operations at Mol. Albert Fabry provided the results of his miniature fission chamber measurements on the absolute source normalization for the power runs, and made available the equivalent fission fluxes derived from the early nickel measurements. Pierre D'hondt provided the results of the later nickel, indium, and aluminum dosimetry measurements also analyzed in this report as well as furnishing the locations of the remaining neptunium measurements the results of which are still outstanding at the time of this documentation. The author is also indebted to all these gentlemen for their patience in responding to all the questions raised by him during the course of this work. Thanks are also due to C. Z. Serpan, Jr., and A. Taboada of the Materials Engineering Branch, Division of Engineering, NRC, and Frank Kam of ORNL for their financial support, interest, and encouragement, and to M. L. Williams of LSU for his helpful discussions on the superposition-synthesis method. Finally, appreciation for the work of Brenda Taylor in the typing and preparation of this report is respectfully acknowledged.

EXECUTIVE SUMMARY

Over the past several years, plant life extension programs have been implemented in many U.S. plants. One method of pressure vessel (PV) fluence rate reduction being used in several of the older reactors involves partial replacement of the oxide fuel with metallic rods in those peripheral assemblies located at critical azimuths. This substitution extends axially over a region that depends on the individual plant design, but covers the most critical PV weld and plate locations which may be subject to pressurized thermal shock. In order to analyze the resulting PV dosimetry using these partial length shield assemblies (PLSA), a relatively simple but accurate method needs to be formulated and qualified that treats the axially asymmetric core leakage.

Accordingly, an experiment was devised and performed at the VENUS critical facility in Mol, Belgium. A modification to the cruciform shaped core was made that mocked up a PLSA geometry in one arm, and the resulting configuration became known as VENUS-3. The outermost five rows in the left (and right) arms of VENUS-3 contained steel in place of fuel from the midplane on down; the upper half of these assemblies as well as all the remaining pins contained fuel without modification.

The method chosen for the calculations is a modification of a flux synthesis procedure often used in more conventional geometry. By decomposing the usual synthesis prescription into two components, one contribution arising from sources lying above the midplane and another from sources lying below, a superposition-synthesis model may be readily formulated which combines the results of four two-dimensional discrete ordinates calculations and two one-dimensional calculations.

The condition that should be met for validity of the method is that, for each component, the flux be separable in the axial and cross-width dimensions over the spatial region where it dominates. In the transport geometry involving sources lying above the midplane, the core periphery is composed entirely of active fuel pins, while in the geometry involving sources below the midplane, the outer five rows contain only steel-filled pins.

To eliminate uncertainties in fission distributions from core-physics calculations, the sources employed in the calculations were based on a measured absolute three-dimensional pin-wise source distribution having an estimated uncertainty of about 5%. Saturated activity measurements in units of $\text{reactions} \cdot \text{s}^{-1} \cdot \text{nucleus}^{-1}$ at full power using $^{56}\text{Ni}(\text{n},\text{p})$, $^{115}\text{In}(\text{n},\text{n}')$, and $^{27}\text{Al}(\text{n},\alpha)$ dosimeters were performed at many locations and levels throughout the VENUS-3 configuration with uncertainties estimated at less than 3%.

Comparisons of calculated and measured results in terms of equivalent fission fluxes are more meaningful in the present application than of saturated activities, however, for they remove some of the dependence of the calculated reaction rates on the dosimeter cross sections and of the measured activities on reaction-dependent parameters. Thus these resulting comparisons tend to become better measures of the accuracy of the calculational model itself, which was the primary goal of this VENUS-3 program.

Comparisons of the equivalent fission fluxes involving all the dosimeters indicate agreement generally to within 5% when proper orientation of the coordinate system used in the synthesis procedure is observed. The method is apparently very accurate (i.e., the agreement lies generally within the measurement uncertainties) for detector locations of greatest concern in PLSA geometries. In particular, the agreement behind the PLSA is comparable to that behind an unmodified assembly. In conclusion, the success of the proposed method bodes well for the accuracy of future analyses of on-line plants using PLSAs.

It is anticipated that a second report describing the experimental details of the measurements will serve as companion documentation to this one and will be furnished by the Studiecentrum voor Kernenergie/Centre d'Etude de l'Energie Nucléaire, Mol, Belgium.

1. INTRODUCTION AND BACKGROUND

Over the past several years, pressurized thermal shock (PTS) programs have become operational at many reactors in the United States. At least two independent methods have been employed to reduce fluence rates and the subsequent rate of accumulation of neutron fluence at the pressure vessel by altering the core-source distribution. The first involves changing the refueling pattern to an in-in-out rotation, rather than out-in-in, at the critical azimuths so that twice-burned fuel now appears in the peripheral assemblies at those azimuths for which accumulated pressure vessel fluences have been the highest. This revised fuel loading scheme typically reduces the core leakage at these azimuths by about a factor of two. For many reactors of moderate age, this reduction is adequate to meet the additional plant-life extension (PLEX) requirements. A second method is being used in several of the older reactors where fluence-rate-reduction factors greater than those afforded by the first method have been deemed necessary. This procedure partially replaces the oxide fuel with metallic rods for those peripheral assemblies again located at the critical azimuths. This substitution extends axially over a region that depends on the individual plant design, but covers in particular the most critical weld locations which are subject to PTS phenomena. The reduction in the fluence rate at the critical pressure vessel locations for the latter case is of the order of a factor of ten, and is due principally to the complete removal of the fission source in the critical peripheral assemblies, which is to be contrasted with only an effective partial removal that exists in the first method.

One older reactor that has been subjected to both methods of core-leakage reduction has been H.B. Robinson Unit 2, which underwent a revised fuel shuffling scheme during cycle 9 and the introduction of partial length shield assemblies (PLSAs) consisting of steel rods for cycle 10 and subsequent cycles. The analysis of cycle 9 using the LEPRICON procedure appears in the literature,¹ and is relatively straightforward. However, the use of the partial length shield assembly (PLSA) introduces a geometrical complication that has not existed in heretofore conventional pressure vessel transport analysis, and a procedure should first be sought that adequately approximates the results of this three-dimensional transport with calculations involving only the one- and two-dimensional codes already in use.

Accordingly, a U.S. Nuclear Regulatory Commission (USNRC) and Belgium agreement was struck which served the needs of both parties: The USNRC, with the approval of the Electric Power Research Institute (EPRI), provided LEPRICON software for the Belgians to use in the dosimetry analysis of their DOEL reactors, while the Belgians provided the VENUS facility and further agreed to perform experiments involving PLSA-type configurations which can serve to benchmark the calculational methods. The USNRC through a contractual agreement with the Oak Ridge National Laboratory (ORNL) would

also provide the results of an analysis of these measurements using some simplified calculational procedure. Both parties would benefit from a successful analysis of the VENUS results in that the USNRC could recommend the procedure to the analyses of H.B. Robinson and other U.S. reactors employing the PLSA concept and Belgium to DOEL-1 which would also qualify as a potential PLSA candidate.

The VENUS facility is located at the Studiecentrum voor Kernenergie/Centre d'Etude de l'Energie Nucléaire (SCK/CEN) in Mol, Belgium. A meeting was arranged at Mol between ORNL and SCK/CEN scientists in January 1987 to discuss modifications to the existing configuration which would allow it to approximate the PLSA geometry and the planning of the experiment. The conclusions drawn from this meeting resulted in a proposed design for VENUS-3 which is characterized by the substitution of steel rods for the fuel over the complete lower half of the peripheral fuel pins in the outermost five rows of two diametrically opposite arms of the cross.^{2,3,4} All structural details were unaltered from those of the earlier VENUS-1 and VENUS-2 configurations. The core, however, was modified to employ 4% enriched ²³⁵U in steel clad pins in the inner zone and 3.3% enriched ²³⁵U in Zircaloy-clad pins in the outer zone. Criticality was to be adjusted by modifying the number and arrangement of the pyrex rods surrounding the core inner baffle.

The measurements consisted of obtaining a relative pin-by-pin, three-dimensional spatial distribution of the fission source over the entire core and then following up with a normalization factor that would link this relative distribution to the absolute distribution existing during the run (or runs) involving the dosimetry exposures. Finally, measured values of the dosimeter reaction rates involving up to four reactions at various axial levels and several horizontal locations throughout the configuration were to be provided. As previously mentioned, ORNL was responsible for the calculations of these reaction rates, and calculated-to-experimental (C/E) comparisons were to be made available in either a joint or separate publication by ORNL and SCK/CEN. Previous analyses of both the VENUS-1 and VENUS-2 experiments concentrated on comparison of the results of several calculational methods involving fission source generation (i.e., predictions of eigenvalues and resulting critical fission source distributions) with both in-core and ex-core measurements.^{5,6} Since the focus of the VENUS-3 experiment is essentially on providing data to test transport methods for calculating ex-core fluence rates, the source description used in the calculations was taken from measurements in order to reduce this possible source of uncertainty to negligible proportions.

In addition to the absolute source,^{a,b} the results of measurements performed with $^{58}\text{Ni}(\text{n},\text{p})$ dosimeters^c in March 1988 and some supplemental nickel measurements performed subsequently,^d all the $^{115}\text{In}(\text{n},\text{n}')$ dosimeter measurements,^{d,e} and the $^{27}\text{Al}(\text{n},\alpha)$ dosimeter measurements^e were used in the analysis presented herein. Although these dosimetry results are still preliminary until final calibration results are available, their accuracy is believed to be better than 3%.^f Only those measurements involving the neptunium fission chambers are missing, but results of the calculations are presented in this report so that they may be directly compared with the measurements when the latter become available.

2. THE VENUS-3 FACILITY AND AVAILABLE MEASURED RESULTS

2.1 GENERAL

The VENUS Critical Facility is a zero-power reactor with a cruciform-shaped core. Because of its modest dimensions, benchmark experiments that involve a mock-up of ex-core geometries are limited in their scope to relatively low attenuations of the core radiation. Since the present application can be characterized as a study of geometric rather than deep-penetration effects, the facility is ideally suited to investigate the three-dimensional effects introduced by PLSA core modification.

2.2 GEOMETRY

The VENUS-3 configuration⁷ is shown in the plan view in Fig. 1. The core consists of three types of fuel pins: stainless-steel-clad UO_2 rods containing 4% enriched ^{235}U , Zircaloy-clad UO_2 rods containing 3.3% enriched ^{235}U , and Zircaloy-clad UO_2 rods containing 3.3% enriched ^{235}U over the upper

^aL. Leenders, SCK/CEN, Mol, Belgium, personal communications to F. B. K. Kam and R. E. Maerker, Oak Ridge National Laboratory, Oak Ridge, Tennessee, August 30, 1988, updated September 8, 1988.

^bA. Fabry, SCK/CEN, Mol, Belgium, personal communication to F. B. K. Kam and R. E. Maerker, Oak Ridge National Laboratory, Oak Ridge, Tennessee, January 13, 1989.

^cA. Fabry, SCK/CEN, Mol, Belgium, personal communication to F. B. K. Kam, Oak Ridge National Laboratory, Oak Ridge, Tennessee, October 19, 1988.

^dP. D'hondt, SCK/CEN, Mol, Belgium, personal communication to F. B. K. Kam and R. E. Maerker, Oak Ridge National Laboratory, Oak Ridge, Tennessee, January 19, 1989.

^eP. D'hondt, SCK/CEN, Mol, Belgium, personal communication to F. B. K. Kam and R. E. Maerker, Oak Ridge National Laboratory, Oak Ridge, Tennessee, February 2, 1989.

half of their height and Zircaloy-clad steel rods over the lower half. The first two types of fuel pins are of uniform composition over their complete height. The 4% enriched rods are positioned in the inner part of the core and occupy the areas designated by the Roman numerals III, IV, and V; the 3.3% enriched rods are located in the arms of the cross at the cross-hatched positions indicated by the Roman numeral II; the PLSA-modified rods are located in two of the arms and are designated by the slanted shading in Fig. 1 and Roman numeral I. Poisons in the form of pyrex pins are located at 44 symmetric locations in the inner core in order to make the reactor critical. The pin-to-pin pitch for all fuel types is 1.26 cm, which is typical of the 17 x 17 lattices in existing pressurized water reactor (PWR) fuel assemblies. In one quadrant of the configuration, a mock-up of the pressure vessel internals representative of a PWR power plant is placed. The inner and outer baffles, core barrel, and neutron pad are all composed of stainless steel, and in addition to the region between the fuel pins, water surrounds the outer baffle, the region between the neutron pad and the core barrel, and the central hole inside the inner baffle.

Measurements of the earlier $^{58}\text{Ni}(\text{n},\text{p})$ reaction rates were performed at the 19 baffle and core barrel locations indicated in Fig. 1 by white squares, as well as at four locations in the PLSA indicated by black squares.^f This range of locations covers regions of different sensitivity to the PLSA geometry, and even includes four locations of virtual zero sensitivity - the two in the inner baffle and the 68° and 89° locations in the core barrel - which can be used to check the simpler calculations involving complete axial symmetry. The locations of the later nickel measurements included five additional positions not indicated in Fig. 1 and the upper part of the axial profiles at the three PLSA centerline locations. The remaining dosimeter measurements introduced no new locations beyond these, and were restricted primarily to the core barrel.

An elevation view of the configuration appears in Fig. 2, which shows the 50-cm-high fuel rods at all locations except in the PLSA region where their effective height is only the 25 cm lying above the reactor midplane. The earlier $^{58}\text{Ni}(\text{n},\text{p})$ reaction rate measurements at each location in Fig. 1 were performed at several axial levels, varying from a minimum of three levels for most of the baffle and core barrel locations to seven levels below midplane in the PLSA region to a maximum of 14 levels at five locations in the core barrel and one location in the outer baffle (see Tables 2 and 3). The indium, aluminum, and neptunium measurements involved either three levels or the full 14 levels.

^fIn actuality, the three PLSA locations indicated in Fig. 1 as lying two squares above the -X axis were located three squares above, but the fluxes at these locations are virtually independent of Y.

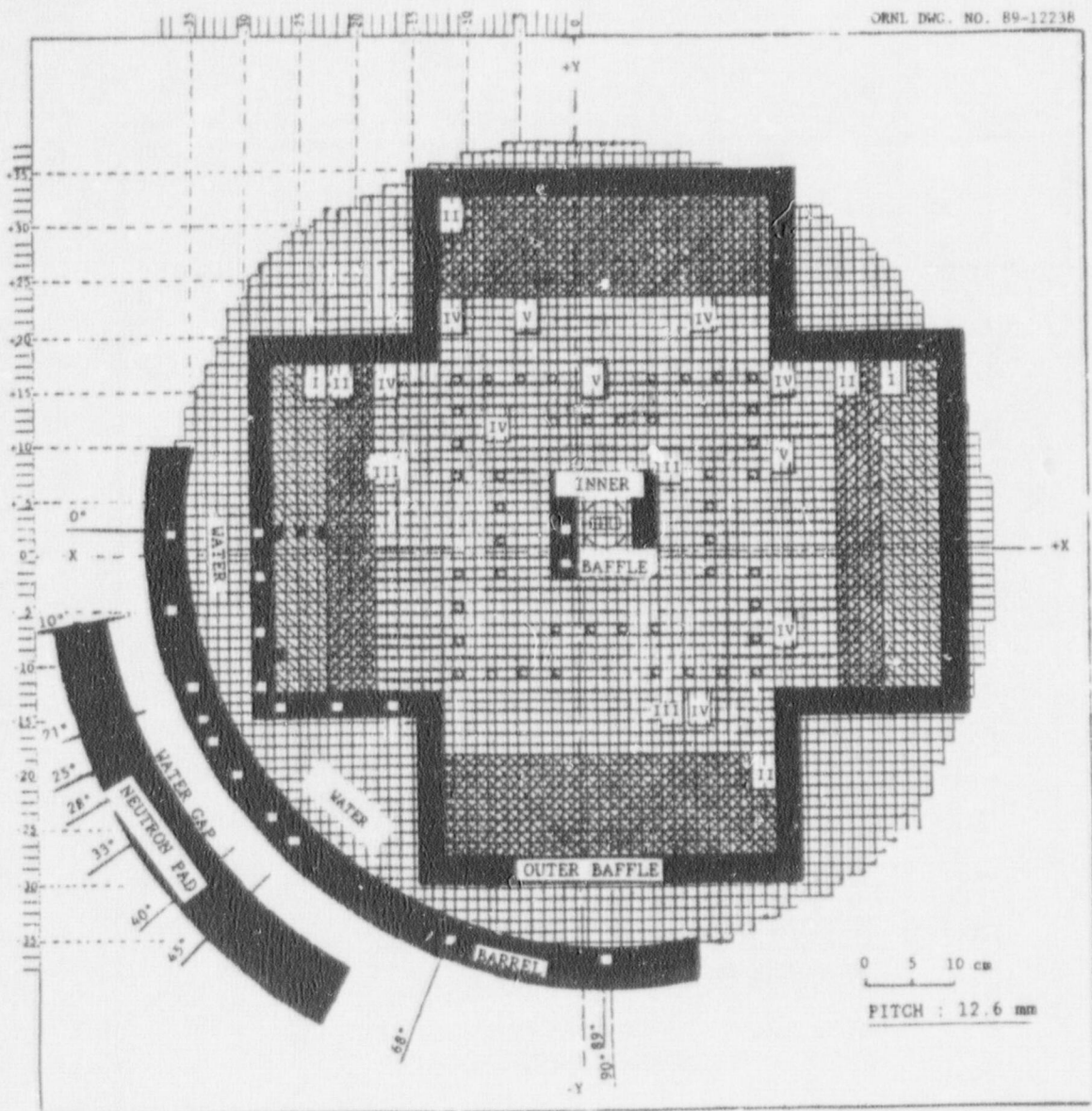


Fig. 1. Plan view of the VENUS-3 facility showing the location of the nickel dosimeters used in the early run of March 1988, and the coordinate system defined by SCK/CEN (see text).

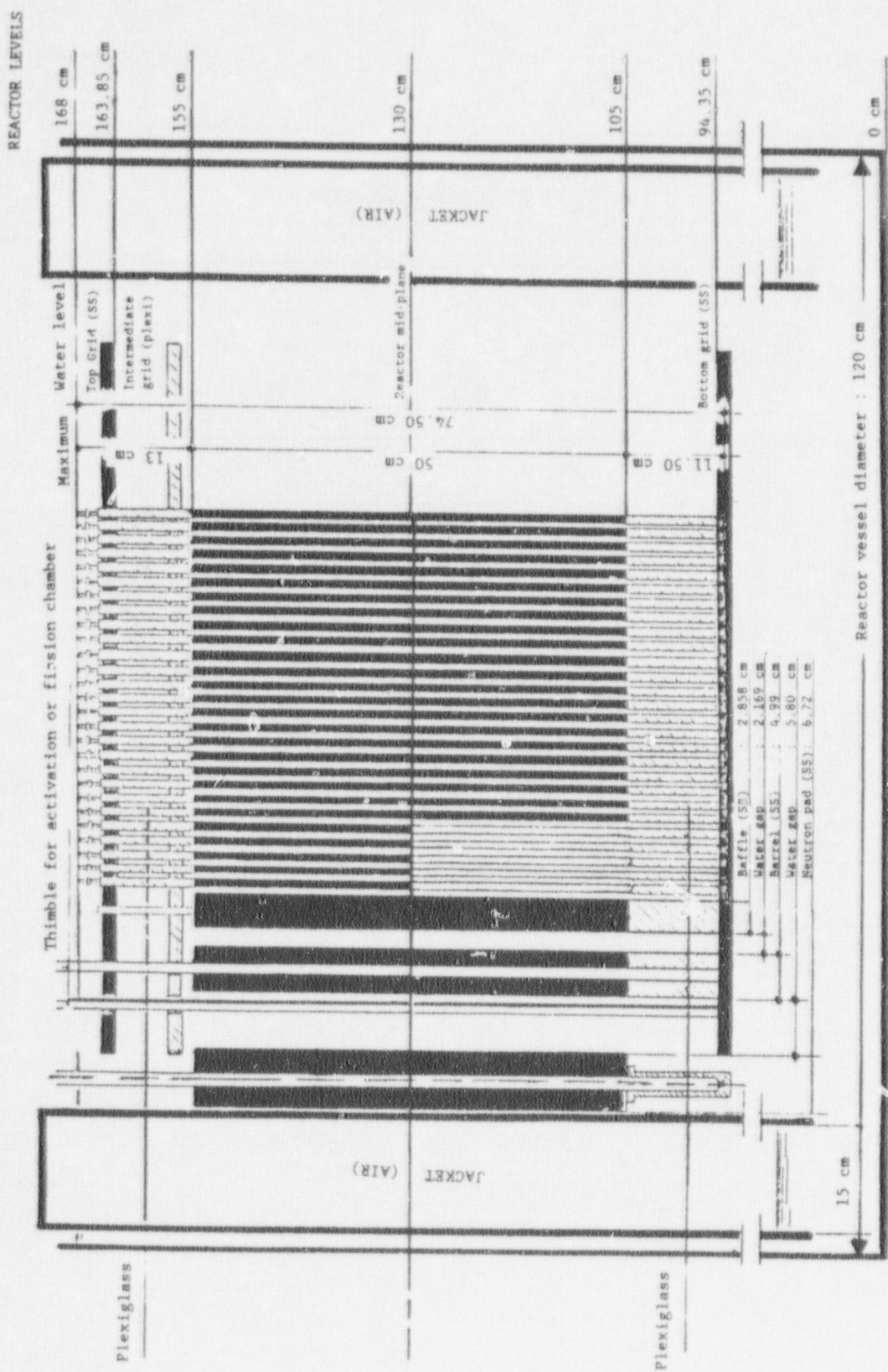


Fig. 2. Elevation view of the VENUS-3 facility showing the substitution of stainless steel rods for oxide fuel in the lower halves of five peripheral pins.

2.3 SOURCE DESCRIPTION

As mentioned in Section 1, the VENUS-3 source was determined experimentally, using a gamma-ray-scanning technique performed on many fuel pins located throughout the core. These three-dimensional relative distributions were obtained at fine enough intervals that interpolation between measured values was estimated to be accurate to within 5% (see Footnote a). The accuracy of the individual measurements was estimated to be 2% (see Footnote a). Enough data (both measured and interpolated) were supplied in Footnote a to produce a complete pin-by-pin radial distribution at two levels: 114.5 cm and 145.5 cm (see Fig. 2), and a complete pin-by-pin radial distribution at all 14 levels between 105 cm and 155 cm for all pin locations in the west-by-southwest octant of the core lying to the left of the 45° direction indicated in Fig. 1. Further interpolation had to be performed at times by ORNL to cover some locations in the left half of the bottom arm and in the core interior that lie to the right of this direction. It is assumed that the source distribution in the lower left quadrant of the core is identical to that in each of the remaining quadrants, i.e., any source perturbations caused by the core barrel and neutron pad are neglected. This is a reasonable assumption, especially for reaction rate measurements performed in the lower left quadrant. The entries for the source distribution appearing in Footnote a are expressed in units of fissions per pin per second, arbitrarily normalized to a core averaged power of one fission per second per active fuel pin. Since there are 639 active pins (including those in the PLSA) in a quadrant of the core, and 2.432 neutrons per thermal fission (proposed value for ENDF/B-VI), this normalization is equivalent to 639 fissions per second or 1554 neutrons per second summed over a quadrant. For this normalization,

$$\rho_{XZ}(\text{n/cm}^2 \cdot \text{s}) = \frac{2.432}{50 \times 1.26} \sum_i \text{entry}(X, Y_i, Z) = 0.03860 \sum_i \text{entry}(X, Y_i, Z), \quad (1)$$

$$\rho_{XY}(\text{n/cm}^2 \cdot \text{s}) = \frac{2.432}{50 \times 1.26^2} \sum_j \text{entry}(X, Y, Z_j) \Delta Z_j = 0.03064 \sum_j \text{entry}(X, Y, Z_j) \Delta Z_j, \quad (2)$$

and

$$\rho_X(\text{n/cm} \cdot \text{s}) = \frac{2.432}{50 \times 1.26} \sum_{ij} \text{entry}(X, Y_i, Z_j) \Delta Z_j = 0.0386 \sum_{ij} \text{entry}(X, Y_i, Z_j) \Delta Z_j, \quad (3)$$

where "entry" in the above equations refers to the actual three-dimensional tabular data transmitted from Belgium, and the two-dimensional neutron source densities ρ have been summed over the third dimension and the one-dimensional source density has been summed over the remaining two dimensions. These densities, when calculated for different ranges of Z , become the source terms to be used in the transport calculations (see Section 3).

An example of the entries in Footnote a is shown in Table 1, where the axial source profiles at the center of the peripheral rows at 0° and 90° are compared. From Fig. 1, the first location corresponds to the left-most blackened square in the middle of the PLSA region, and the second location corresponds to the midpoint of the outside row in the lower arm of the unmodified region.

Table 1. Comparison of source profiles at corresponding locations in the PLSA and unmodified regions*

PLSA	Z level (cm)	Unmodified
0.0	106.5	0.40958
0.0	110.5	0.40750
0.0	114.5	0.51246
0.0	118.5	0.60219
0.0	122.5	0.65354
0.0	125.5	0.70031
0.0	128.5	0.71274
0.50132	131.5	0.71547
0.50221	134.5	0.70114
0.51098	137.5	0.67705
0.48107	141.5	0.61180
0.43399	145.5	0.53342
0.36044	149.5	0.42022
0.35777	153.5	0.40554

*Units are fissions per pin per second. The average pin powers are 0.22253 and 0.56545, respectively.

It is observed that the absence of fuel below the reactor midplane in the modified assembly reduces the source above the midplane by between 12% and 30%.

2.4 ABSOLUTE SOURCE NORMALIZATION

The reaction rate measurements to be presented next have been normalized to "100% VENUS-3 power." Preliminary absolute measurements of the core fission rates at several locations using ^{235}U miniature fission chambers yielded a value of $8.845 \times 10^9 \pm 4\%$ as the multiplication factor for converting the arbitrarily normalized source employed in the calculations to the source at 100% power.⁸

Before presenting the results of the reaction rate measurements, the coordinate system established by Mol in Fig. 1 to locate all detectors will be described. The origin of the Cartesian system is located in the inner baffle at a point 2.5 pitches (3.5 cm) to the left and 2.5 pitches below the geometric center of the core. The southwest quadrant of the core is thus defined by the ranges $-27 \leq X \leq +2$ and $-27 \leq Y \leq +2$, where the limits represent cell center-to-center distances in units of pitches. Positions exterior to the core may also be located by extending the grid to include the outer baffle, core barrel, and intervening water. (Note, however, that the baffles are 2.268 pitches thick.)

2.5 RESULTS OF THE EQUIVALENT FISSION FLUX MEASUREMENTS

Tables 2 and 3 present the earlier measured $^{58}\text{Ni}(\text{n},\text{p})$ reaction rates in units of nickel equivalent fission flux at 100% core power. The inner baffle (I.B.), PLSA, and outer baffle (O.B.) data appear in Table 2 and the core barrel (C.B.) data in Table 3. Table 4 presents the results of the supplementary nickel measurements. It is to be observed that one of the new locations is in the water gap about halfway between the core barrel and the outer baffle at 0° . The locations and results for the indium measurements appear in Table 5 and for aluminum in Table 6. The remaining dosimeters for which data are not yet available and the locations at which the measurements were made or are anticipated are indicated in Table 7. The locations of the ^{235}U fission chamber measurements are included only for completeness, as they will not be analyzed by ORNL.

⁸A value of 5.652×10^{12} fissions per second per core quadrant was quoted in Footnote b as corresponding to 100% power. Dividing by 639 fissions per second assumed for the arbitrary normalization per quadrant results in the factor above.

Table 2. Measured nickel equivalent fission fluxes at 100% power
at all locations except the core barrel

Location	Axial level (cm)	Flux	Location	Axial level (cm)	Flux
I.B. -1/+2	114.5	1.233+9*	I.B. -1/-1	114.5	1.474+9
	131.45	1.743+9		131.45	2.086+9
	131.55	1.760+9		131.55	2.097+9
	145.5	1.248+9		145.5	1.523+9
PLSA -27/+3	106.5	1.648+8	PLSA -25/+3	106.5	2.713+8
	110.5	2.296+8		110.5	3.843+8
	114.5	2.947+8		114.5	4.896+8
	118.5	3.548+8		118.5	5.899+8
	122.5	4.275+8		122.5	6.947+8
	125.5	5.062+8		125.5	7.980+8
	128.5	6.752+8		128.5	1.025+9
PLSA -23/+3	106.5	5.115+8	PLSA -27/-9	106.5	1.141+8
	110.5	7.161+8		110.5	1.480+8
	114.5	9.113+8		114.5	1.793+8
	118.5	1.094+9		118.5	2.212+8
	122.5	1.264+9		122.5	2.646+8
	125.5	1.400+9		125.5	3.204+8
	128.5	1.624+9		128.5	1.460+8
O.B. -29/+2	106.5	9.802+7	O.B. -29/-2	114.5	1.636+8
	110.5	1.360+8		131.5	4.639+8
	114.5	1.750+8		145.5	4.638+8
	118.5	2.106+8	O.B. -29/-7	114.5	1.362+8
	122.5	2.576+8		131.5	3.803+8
	125.5	3.085+8		145.5	3.778+8
	128.5	3.880+8	O.B. -29/-12	114.5	9.002+7
	131.5	5.003+8		131.5	2.211+8
	134.5	5.571+8		145.5	2.157+8
	137.5	5.731+8	O.B. -27/-14	114.5	1.059+8
	141.5	5.544+8		131.5	2.395+8
	145.5	4.945+8		145.5	2.220+8
	149.5	4.052+8	O.B. -22/-14	114.5	3.080+8
	153.5	2.912+8		131.5	5.194+8
				145.5	4.341+8
			O.B. -17/-14	114.5	6.242+8
				131.5	9.238+8
				145.5	7.106+8

*Read as 1.233×10^9 n/cm²·s.

Table 3. Measured nickel equivalent fission fluxes at 100% power
at the core barrel locations

Angle	Location	Axial level (cm)	Flux	Angle	Location	Axial level (cm)	Flux
0°	C.B. -37/+2	106.5	1.694+7*	21°	C.B. -35/-12	106.5	1.415+7
		110.5	2.221+7			110.5	1.923+7
		114.5	2.824+7			114.5	2.383+7
		118.5	3.597+7			118.5	2.960+7
		122.5	4.388+7			122.5	3.559+7
		125.5	4.936+7			125.5	4.042+7
		128.5	5.539+7			128.5	4.540+7
		131.5	6.090+7			131.5	5.030+7
		134.5	6.453+7			134.5	5.411+7
		137.5	6.676+7			137.5	5.520+7
		141.5	6.438+7			141.5	5.348+7
		145.5	5.873+7			145.5	4.780+7
		149.5	4.932+7			149.5	4.042+7
		153.5	3.757+7			153.5	3.071+7
45°	C.B. -26/-26	106.5	1.749+7	68°	C.B. -12/-35	106.5	3.421+7
		110.5	2.249+7			110.5	4.652+7
		114.5	2.743+7			114.5	5.720+7
		118.5	3.162+7			118.5	6.502+7
		122.5	3.529+7			122.5	7.095+7
		125.5	3.743+7			125.5	7.478+7
		128.5	3.848+7			128.5	7.515+7
		131.5	3.864+7			131.5	7.681+7
		134.5	3.843+7			134.5	7.491+7
		137.5	3.811+7			137.5	7.236+7
		141.5	3.508+7			141.5	6.641+7
		145.5	3.090+7			145.5	5.715+7
		149.5	2.545+7			149.5	4.667+7
		153.5	1.674+7			153.5	3.445+7

*Read as 1.694×10^7 n/cm².s.

Table 3. Continued

Angle	Location	Axial level (cm)	Flux	Angle	Location	Axial level (cm)	Flux
89°	C.B. +2/-37	106.5	4.321+7	10°	C.B. -37/-5	114.5	2.486+7
		110.5	5.814+7			131.5	5.210+7
		114.5	7.080+7			145.5	5.039+7
		118.5	8.203+7	25°	C.B. -34/-15	114.5	2.187+7
		122.5	8.938+7			131.5	4.348+7
		125.5	9.403+7			145.5	4.092+7
		128.5	9.540+7			114.5	2.108+7
		131.5	9.618+7			131.5	3.942+7
		134.5	9.429+7			145.5	3.673+7
		137.5	9.057+7	33°	C.B. -31/-20	114.5	2.880+7
		141.5	8.207+7			131.5	4.480+7
		145.5	7.174+7			145.5	3.927+7
		149.5	5.807+7	40°	C.B. -28/-24	114.5	2.534+7
		153.5	4.317+7			131.5	3.764+7
						145.5	3.059+7

*Read as 1.694×10^7 n/cm².s.

Table 4. Locations and results for measured supplemental nickel equivalent fission fluxes at 100% power

Location	Axial level (cm)	Flux	Location	Axial level (cm)	Flux	Location	Axial level (cm)	Flux
PLSA -27/+2	131.05	1.084+9*	PLSA -25/+3	131.05	1.617+9	PLSA -23/+2	131.05	2.280+9
	134.15	1.234+9		134.15	1.846+9		134.15	2.426+9
	137.25	1.280+9		137.25	1.897+9		137.25	2.443+9
	141.35	1.227+9		141.35	1.846+9		141.35	2.309+9
	145.45	1.108+9		145.45	1.628+9		145.45	2.030+9
	149.55	9.125+8		149.55	1.354+9		149.55	1.656+9
	153.65	7.026+8		153.65	1.033+9		153.65	1.250+9
3.3% Fuel -21/+2	106.05	9.316+8	3.3% Fuel -19/+3	106.05	1.141+9	3.3% Fuel +2/+23	106.05	1.285+9
	110.15	1.282+9		110.15	1.589+9		110.15	1.768+9
	114.25	1.644+9		114.25	2.014+9		114.25	2.210+9
	118.35	1.986+9		118.35	2.424+9		118.35	2.606+9
	122.45	2.276+9		122.45	2.774+9		122.45	2.898+9
	125.55	2.494+9		125.55	2.988+9		125.55	3.045+9
	128.65	2.683+9		128.65	3.160+9		128.65	3.120+9
	131.75	2.860+9		131.75	3.267+9		131.75	3.118+9
	134.85	2.925+9		134.85	3.295+9		134.85	3.047+9
	137.95	2.855+9		137.95	3.218+9		137.95	2.894+9
	141.05	2.744+9		141.05	3.046+9		141.05	2.706+9
	145.15	2.406+9		145.15	2.679+9		145.15	2.333+9
	149.25	1.967+9		149.25	2.195+9		149.25	1.888+9
	153.35	1.473+9		153.35	1.651+9		153.35	1.403+9
3.3% Fuel -22/+0	106.05	7.661+8	Water Gap -33/+2	106.5	3.736+7			
	110.15	1.057+9		110.5	5.027+7			
	114.25	1.350+9		114.5	6.366+7			
	118.35	1.620+9		118.5	7.684+7			
	122.45	1.876+9		122.5	9.566+7			
	125.55	2.067+9		125.5	1.124+8			
	128.65	2.280+9		128.5	1.330+8			
	131.75	2.527+9		131.5	1.509+8			
	134.85	2.628+9		134.5	1.646+8			
	137.95	2.622+9		137.5	1.680+8			
	141.05	2.495+9		141.5	1.636+8			
	145.15	2.209+9		145.5	1.448+8			
	149.25	1.829+9		149.5	1.207+8			
	153.35	1.376+9		153.5	8.650+7			

*Read as 1.084×10^9 n/cm²·s.

Table 5. Locations and results for the measured indium equivalent fission fluxes at 100% power

Axial level (cm)	Angle	Location	Flux	Angle	Location	Flux	Angle	Location	Flux
106.5	0, B, -29/+2	1, 189+8*			Water Gap	3, 767+7	33°	C, B, -31/-20	1, 696+7
110.5		1, 698+8	-33/+2		5, 187+7				2, 323+7
114.5		2, 181+8			6, 610+7				2, 886+7
118.5		2, 657+8			8, 268+7				3, 446+7
122.5		3, 256+8			9, 990+7				3, 955+7
125.5		3, 871+8			1, 187+8				4, 336+7
128.5		4, 859+8			1, 405+8				4, 677+7
131.5		6, 112+8			1, 553+8				4, 954+7
136.5		6, 915+8			1, 725+8				5, 079+7
137.5		7, 196+8			1, 835+8				5, 121+7
141.5		6, 896+8			1, 786+8				4, 861+7
145.5		6, 182+8			1, 596+8				4, 393+7
149.5		5, 062+8			1, 366+8				3, 866+7
153.5		3, 614+8			1, 003+8				2, 700+7
116.5	10°	C, B, -37/-5	3, 116+7	21°	C, B, -35/-12	3, 145+7	40°	C, B, -28/-24	2, 928+7
131.5		6, 647+7			6, 527+7				4, 4557+7
145.5		6, 490+7			6, 317+7				3, 611+7
114.5	45°	C, B, -26/26	3, 187+7	68°	C, B, -12/-35	7, 292+7	25°	C, B, -34/-15	2, 916+7
131.5		4, 601+7			1, 001+8				5, 782+7
145.5		3, 651+7			7, 480+7				5, 406+7
106.5	0°	C, B, -37/+2	1, 898+7	28°	C, B, -33/-17	1, 616+7	89°	C, B, +2/-37	5, 576+7
110.5		2, 632+7			2, 251+7				7, 180+7
114.5		3, 366+7			2, 843+7				8, 627+7
118.5		4, 168+7			3, 422+7				9, 990+7
122.5		5, 081+7			4, 037+7				1, 101+8
125.5		5, 862+7			4, 450+7				1, 140+8
128.5		6, 611+7			4, 936+7				1, 168+8
131.5		7, 527+7			5, 326+7				1, 159+8
134.5		7, 857+7			5, 578+7				1, 156+8
137.5		8, 181+7			5, 706+7				1, 111+8
141.5		7, 946+7			5, 482+7				1, 006+8
145.5		7, 187+7			4, 892+7				8, 685+7
149.5		6, 076+7			4, 325+7				7, 624+7
153.5		4, 538+7			3, 061+7				5, 050+7
131.5	1, B, -1/+2	2, 249+9		I, B, -1/-1	2, 713+7				

*Read as 1.189×10^8 n/cm².s.

Table 6. Locations and results for the measured aluminum equivalent fission fluxes at 100% power

Axial level (cm)	Angle	Location	Flux	Angle	Location	Flux	Angle	Location	Flux	
114.5	0, B.	-29/+2	1.852+8*		Water Gap -33/+2	8.376+7 1.871+8	0°	C, B.	-37/+2	
131.5			4.788+8			1.782+8			4.110+7 7.669+7	
145.5			4.765+8						7.270+7	
114.5	10°	C, B.	-37/-5	21°	C, B.	-35/-12	25°	C, B.	-34/-15	
131.5			3.197+7			3.159+7			3.051+7	
145.5			6.316+7			6.022+7			5.328+7	
			6.026+7			5.705+7			4.801+7	
114.5	28°	C, B.	-33/-17	2.753+7	33°	C, B.	-31/-20	40°	C, B.	-28/-24
131.5			4.977+7			3.168+7			3.683+7	
145.5			4.330+7			5.149+7			5.481+7	
						4.350+7			4.279+7	
114.5	45°	C, B.	-26/-26	3.807+7	68°	C, B.	-12/-35	89°	C, B.	+2/-37
131.5			5.532+7			6.806+7			9.554+7	
145.5			4.231+7			8.915+7			1.202+8	
						6.547+7			8.848+7	
131.5		I, B.	-1/-1	1.927+9		I, B.	-1/+2		1.561+9	

*Read as $1.852 \times 10^8 \text{ n/cm}^2 \cdot \text{s}$.

Table 7. Remaining dosimeters and their locations

Fission chamber traverses at 14 levels*

^{237}Np O.B. -29/+2
 W.G. -33/+2
 Barrel 0°, 10°, 21°, 25°, 28°, 33°, 40°, 45°, 68°, 89°

^{235}U O.B. -29/+2
 W.G. -33/+2
 Barrel 0°, 10°, 21°, 25°, 28°, 33°, 40°, 45°, 68°, 89°

*in cm: 106.5, 110.5, 114.5, 118.5, 122.5, 125.5, 128.5, 131.5, 134.5,
 137.5, 141.5, 145.5, 149.5, 153.5

3. DESCRIPTION OF THE CALCULATIONS

3.1 FLUX SUPERPOSITION-SYNTHESIS MODEL

A method for approximating neutron transport in three dimensions by combining the results of several lower dimensional calculations has been in use for at least seven years now.^b This deceptively simple method is exact whenever the flux is separable in either Y or Z, X being the direction of principal flow (or θ or Z, R being the direction of principal flow), and may be written, for example, as

$$\phi_b(X, Y, Z) = \phi_b(X, Y)\phi_b(X, Z)/\phi_b(X), \quad (4)$$

where the source normalizations for each of the channel flux calculations on the R.H.S. of Eq. (4) may be obtained from

$$S_b(X, Y) = \int_Z S_b(X, Y, Z) dZ , \quad (5)$$

$$S_b(X, Z) = \int_Y S_b(X, Y, Z) dY , \quad (6)$$

$$\text{and } S_b(X) = \int_Y dY \int_Z S_b(X, Y, Z) dZ . \quad (7)$$

The effects of finite core height may be accurately taken into account without resorting to three-dimensional calculations or employing artificial buckling corrections by using Eqs. (4) through (7) for fluxes confined to a region defined by the reactor beltline. There should exist only small changes in the geometry in the Y or Z directions, of course, for this approximation to remain valid. When the source varies significantly with Z, for example, the method as presented has a more limited range of validity. This is the case in PLSA-modified geometries, where the peripheral source has a discontinuity and, in addition, there is a medium change in the peripheral assemblies between the upper and lower pin regions.

A modification to Eqs. (4) through (7), introduced by M. L. Williams, has been adopted to aid in the assessment of flux-reduction factors afforded by possible PLSA configurations in H.B. Robinson Unit 2.⁸ By decomposing the synthesis prescription of Eq. (4) into two components, one contribution

^bThe author was first introduced to this idea through a suggestion made by J. Cavanaugh of Combustion Engineering, Inc., Windsor, Connecticut. It has subsequently been refined by J. J. Wagschal of the Hebrew University, Jerusalem, Israel, and M. L. Williams of Louisiana State University, Baton Rouge, Louisiana.

arising from sources (A) lying above the midplane and another from sources (B) lying below, Eq. (4) becomes

$$\phi_g(X, Y, Z) = \frac{\phi_g^A(X, Y, Z)}{\phi_g^A(X)} + \frac{\phi_g^B(X, Y, Z)}{\phi_g^B(X)} \quad (8)$$

Equation (8) represents the superposition-synthesis model proposed for the VENUS-3 analysis.

The sources to be used in the VENUS-3 flux calculations are

$$S_g^A(X, Y) = \int_{130}^{155} S_g(X, Y, Z) dZ \quad , \quad (9)$$

$$S_g^A(X, Z) = \int_{-\infty}^{\infty} S_g(X, Y, Z \geq 130) dY \quad , \quad (10)$$

$$S_g^A(X) = \int_{-\infty}^{\infty} dY \int_{130}^{155} S_g(X, Y, Z) dZ \quad , \quad (11)$$

$$S_g^B(X, Y) = \int_{105}^{130} S_g(X, Y, Z) dZ \quad , \quad (12)$$

$$S_g^B(X, Z) = \int_{-\infty}^{\infty} S_g(X, Y, Z \leq 130) dY \quad , \quad (13)$$

$$S_g^B(X) = \int_{-\infty}^{\infty} dY \int_{105}^{130} S_g(X, Y, Z) dZ \quad , \quad (14)$$

$$\text{and } \int_{-34.65}^{3.15} S_g^A(X) dX + \int_{-34.65}^{3.15} S_g^B(X) dX = S_g^A + S_g^B = 3.108 \times 10^3 \text{ n/s over } \frac{1}{2} \text{ core.} \quad (15)$$

The condition to be met now is that, for each source component, the flux be separable in Y or Z over the spatial extent where it dominates, which is far less restrictive than before. In the transport geometry using sources defined by Eqs. (9) and (11), the core periphery is made up exclusively of 3.3% fuel pins, while in the geometry using sources defined by Eqs. (12) and (14), the periphery contains only the stainless-steel-filled pins. These choices are dictated by the fact that the neutron transmission properties of the fuel and the stainless steel regions are nearly the same (see Table 6), and hence the medium through which the major contribution to the core leakage from each source component passes is the one nearest the source. There is, however, a cross-over point below the midplane above which the contribution from the upper part of the PLSA still dominates the ex-core flux. The location of this point is physically the most interesting problem to be solved (see Fig. 3).

Table 8. Neutron transmission through UO_2 relative to stainless steel in the VENUS-3 PLSA geometry*

Reaction	$T_{\text{UO}_2}/T_{\text{SS}}^{**}$	Reaction	$T_{\text{UO}_2}/T_{\text{SS}}^{**}$
$^{63}\text{Cu}(\text{n},\alpha)$	1.050	$^{46}\text{Ti}(\text{n},\text{p})$	1.054
$^{32}\text{S}(\text{n},\text{p})$	1.039	$^{54}\text{Fe}(\text{n},\text{p})$	1.040
$^{58}\text{Ni}(\text{n},\text{p})$	1.033	$^{238}\text{U}(\text{n},\text{f})$	0.991
$^{115}\text{In}(\text{n},\text{n}')$	0.980	$^{103}\text{Rh}(\text{n},\text{n}')$	0.952
$^{237}\text{Np}(\text{n},\text{f})$	0.937	$\phi > 1 \text{ MeV}$	0.956
dpa	0.957	$\phi > 0.1 \text{ MeV}$	0.925

*Identical core source distribution assumed for each one-dimensional calculation. The thickness of the UO_2 or stainless steel penetration is 6.3 cm.

**Average of several locations in the outer baffle.

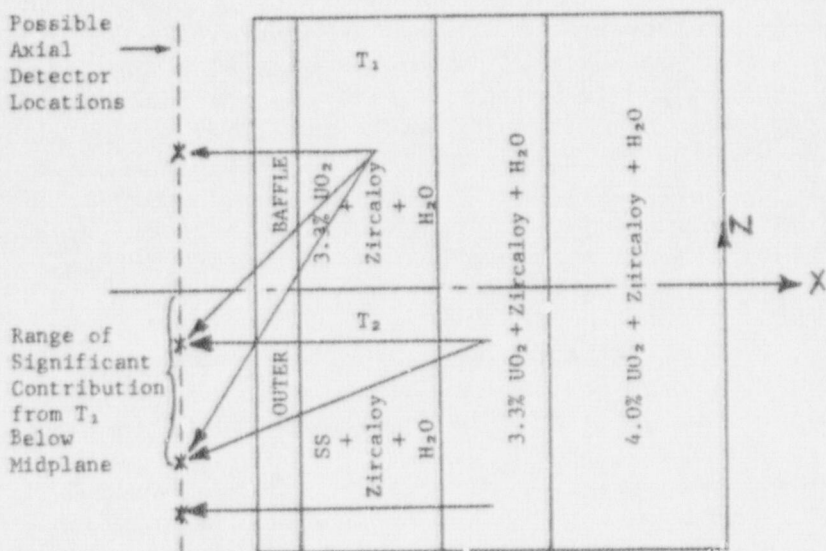


Fig. 3. Illustrating the region where the flux superposition-synthesis procedure may break down if the relative transmissions of the upper and lower peripheral core media are significantly different. (They are not for VENUS-3.)

However, in actual PLSA applications, the length of the shield section of the assembly is selected such that the critical location in the RPV is sensitive mainly to the reduced source geometry (i.e., in the lower axial region in this case).

3.2 MODELING OF THE VENUS-3 GEOMETRY

A fundamental question arises immediately as to whether to employ X-Y or R- θ coordinates in the horizontal cross section description of VENUS-3. It was rather easily decided to use a Cartesian system for the following reasons. The first is that an accurate description of the core and baffles seems more important than an accurate description of the core barrel and neutron pad (i.e., most of the transport involves X-Y geometry whereas the neutron pad, intervening water gap, and part of the core barrel serve primarily to reflect neutrons). The second is that the source is described in Cartesian coordinates, and source manipulations necessary to change it to cylindrical coordinates with consequent partial summations over these variables would compromise the accuracy of the original data. It should be noted that the adoption of the X-Y-Z system to describe the VENUS-3 geometry in the transport calculations is at variance with the R- θ -Z system used in conventional LWR analysis. However, the focus of the experiment is on the validation of an analytic procedure to use in PLSA-modified geometries, and obviously the procedure should lend itself equally well to either coordinate system.

The X-Y geometry was set up using the variable mesh option available in the standard two-dimensional discrete ordinates transport code DOT 4.⁹ There were 65 X intervals and between 36 and 101 Y intervals to describe the geometry that included that half of the core containing the PLSA, the core barrel, and the neutron pad to beyond the neutron pad (see Fig. 4). The orientation of Fig. 4 is such that it represents the geometry in Fig. 1 which has been rotated 90° clockwise so that the PLSA assembly is situated in the upper arm. The representation of the curved boundaries of the core barrel, neutron pad, and the jacket inner wall are well described by the variable mesh option and there should be negligible error introduced in the transport results arising from the stair-step approximations to the curvilinear geometry. A reflection condition was imposed along the x axis appearing in Fig. 4, but the inclusion of the 180° geometry permits asymmetrical fluxes to be calculated on either side of the y axis although the corresponding sources were assumed to be symmetrical (see Section 2).

The X-Z and X geometries were straightforward. The X-Z description employed a fixed mesh of 77 Z intervals along with the previously established 65 X intervals, using a geometry taken from a preliminary version of Ref. 7. The height of these Z intervals was 1 cm within the active core, to permit accurate definition of the axial profiles. The minor differences between the axial specifications presented in Ref. 7 and those in the X-Z geometry used in the calculations involve components lying beyond the dimensions of the active core, and may be safely disregarded.

HORIZONTAL PLANE (X-Y) GEOMETRY FOR VENUS-3

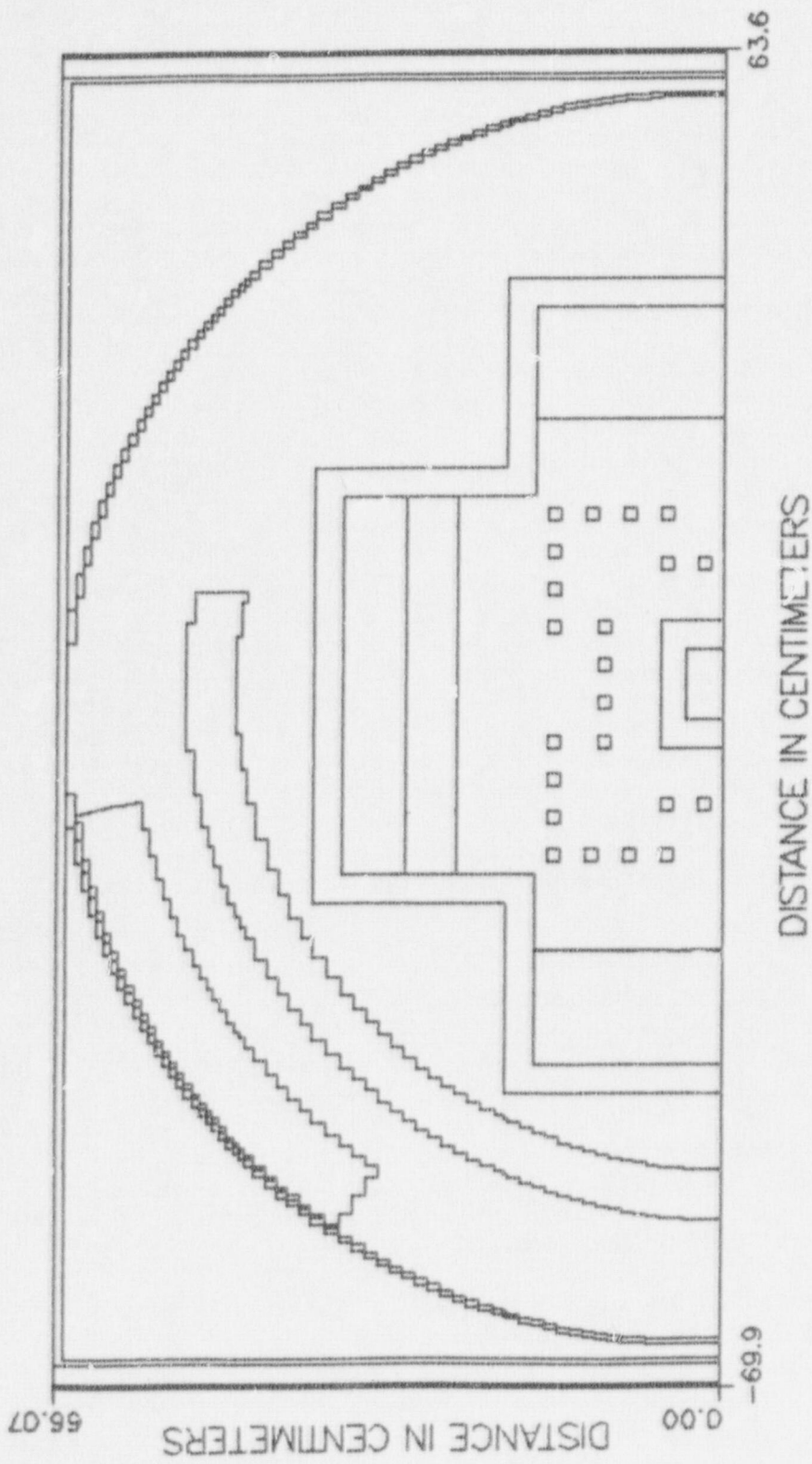


Fig. 4. Plan view of the VENUS-3 facility as defined using the variable mesh option with X-Y geometry in DOT-4. The X axis is now the vertical axis and the PLSA is located in the upper arm of the cross (see text.)

The X geometry consisting of the 65 X intervals was used in ANISN,¹⁰ a one-dimensional discrete ordinates transport code, rather than in the one-dimensional mode available in DOT 4.

The calculations described so far involve an X-Y run, an X-Z run, and an X run, all for each of the two source components, for a total of six discrete ordinates calculations. The two one-dimensional runs, of course, require very little CPU time, so that the four two-dimensional runs dominate the computing effort. It is to be expected, however, that the two measurements in the core barrel at 68° and 89° [or any such similar locations requiring a considerable reorientation of the coordinate system defined in Eqs. (8) through (14) and Fig. 1] may not be well calculated. It should be recalled that the significance of the X and Y axes in Eqs. (8) through (14) is in their interpretation as parallel and perpendicular to the principal direction of flow to the flux point, respectively. This direction can be approximated in the present geometry by a line joining the center of the core with the flux point (i.e., the detector) in question. For most of the detectors shown in Fig. 1, the detector-independent X-Y coordinate system defined in Fig. 1 is assumed to be adequate. For detectors at angles greater than 45° with the X axis, X and Y may be interchanged in Eqs. (8) through (15) and the sources resummed. This has no effect on the X-Y transport calculations if X and Y are reinterpreted as the old Y and X, and the original results are still valid. The X-Z and X transport calculations must be redone, however, since their source terms are now different. This results in additional X-Z and X runs for each of the two source components. A grand total of ten discrete ordinates calculations were thus made. The reaction rates at 68° and 89° that were calculated using the re-oriented coordinate system provide a good reference point for confirming the accuracy of the synthesis procedure in the vicinity of an unmodified assembly, where no consideration of axial source components (i.e., superposition) is necessary.

3.3 SOME DETAILS OF THE CALCULATIONS

Cross sections used in the transport calculations as well as in the calculation of the dosimetry responses were based on the ELXSIR¹¹ library which is part of the LEPRICON system. The iron cross sections were based on updates of Mod 3 of ENDF/B-V, a superior evaluation due to Fu and Hetrick.¹² Flux calculations were extended down through group 38 (0.098 MeV) which is adequate to cover the range of responses for all dosimetry anticipated. (The ²³⁵U measurements were not analyzed by ORNL.)

Table 9 summarizes the values assigned to the more important parameters input to the discrete ordinates codes.

Table 9. Values of some discrete ordinates parameters
input to DOT 4 and ANISN

Parameter	X-Y	X-Z	Parameter	X
ISCTM	3	3	ISCT	3
IZM	17	22	ISN	8
IM	-101	77	IGE	1
JM	65	65	IBL	1
IGM	38	38	IBR	0
IHT	5	5	IZM	14
IHS	6	6	IM	65
IHM	61	61	IGM	38
MTM	41	53	IHT	5
IDFAC	0	0	IHS	6
MM	48	48	IHM	61
INGEOM	0	0	MTP	41
IBL	0	0	MT	41
IBR	0	0	IDFM	0
IBB	1	1	IQM	1
IBT	0	0	IPM	0
IFXMI	30	30	IPP	0
MODE	5	5	IIM	50
KTYPE	0	0	ID1	0
IACC	2	2	ID2	1
INPFXM	0	0	ID3	8
INPSRM	2	2	ID4	1
IACT	8	8	IDAT1	1
IRED	17	22	IFLU	3
NOFIS	2	2		
MSTMAX	1	1		

3.4 RESULTS OF THE CALCULATIONS

Tables 10 through 15 present the results of the calculations for nickel, indium, and aluminum using the source distribution originally normalized to a core-averaged pin power of 1 fission per second. Comparisons of the absolute values of the calculations and measurements will be deferred until Section 4 for those dosimeters for which measurements are available. The calculations for the neptunium dosimeter appear in the appendix.

Table 10. Calculated nickel reaction rate components at locations in the inner baffle and PLSA*

Location	Axial level (cm)	A_{RXY}	A_{RXZ}	A_{RXYZ}	B_{RXY}	B_{RXZ}	B_{RXYZ}	R_{A+B}	R_{B+A}	$R_{XYZ/RXYZ}$
I, B, -1/+2	114.5	4.42-25†	6.46-23	6.18-26	4.22-28‡	4.24-25	6.28-23	2.14-24	1.44-26‡	1.48-26‡
	131.5		2.12-24	1.45-26				9.66-25	6.51-27	2.10-26
	145.5		2.21-24	1.51-26				6.03-26	4.06-28	1.55-26
I, B, -1/-	6.5	5.33-25	6.46-23	6.18-26	5.10-28	5.13-25	6.28-23	2.14-24	1.74-26	1.79-26
	111.5		2.12-24	1.75-26				9.66-25	7.88-27	2.54-26
	145.5		2.21-24	1.83-26				6.03-26	4.92-28	1.88-26
PLSA -27/+2	106.5	3.40-25	1.19-23	5.22-27	1.49-28	1.00-25	4.07-24	6.96-26	1.71-27	1.96-27
	110.5		9.70-27	2.78-28				9.81-26	2.41-27	2.69-27
	114.5		1.77-26	5.08-28				1.19-25	2.92-27	3.43-27
PLSA -25/-2	118.5		3.26-26	9.33-28				1.32-25	3.24-27	4.18-27
	122.5		6.10-26	1.75-27				1.33-25	3.28-27	5.03-27
	125.5		1.01-25	2.90-27				1.26-25	3.04-27	5.96-27
PLSA -23/+2	128.5		1.83-25	5.23-27				1.00-25	2.67-27	7.70-27
	110.5	5.06-25	1.74-23	6.28-27	1.82-28	1.65-25	6.48-24	1.13-25	2.87-27	3.06-27
	114.5		1.15-26	3.35-28				1.62-25	4.13-27	4.46-27
PLSA -23/-2	118.5		2.12-26	6.15-28				1.97-25	5.02-27	5.63-27
	122.5		3.98-26	1.16-27				2.21-25	5.63-27	6.79-27
	125.5		7.65-26	2.22-27				2.27-25	5.80-27	8.02-27
PLSA -27/-9	128.5		1.32-25	3.83-27				2.13-25	5.42-27	9.25-27
	110.5		2.54-25	7.39-27				1.70-25	4.35-27	1.17-26
	114.5		7.35-27	2.12-28	3.18-25	1.19-23	2.15-25	5.74-27	5.95-27	0.964
PLSA -27/-9	118.5		1.37-26	3.95-28				3.04-25	8.12-27	8.52-27
	122.5		2.58-26	7.46-28				3.75-25	1.00-26	1.08-26
	125.5		4.91-26	1.42-27				4.28-25	1.14-26	1.29-26
PLSA -27/-9	128.5		9.59-26	2.77-27				4.51-25	1.21-26	1.48-26
	110.5		1.67-25	4.82-27				4.36-25	1.16-26	1.65-26
	114.5		3.26-25	9.40-27				3.57-25	9.55-27	1.90-26
PLSA -27/-9	118.5		2.23-25	1.19-23	5.22-27	9.79-29	6.92-26	4.07-24	6.96-26	1.18-27
	122.5		9.70-27	1.82-28				9.81-26	1.67-27	1.85-27
	125.5		1.77-26	3.33-28				1.19-25	2.02-27	2.35-27
PLSA -27/-9	128.5		3.26-26	6.11-28				1.32-25	2.24-27	2.85-27
	110.5		6.10-26	1.14-27				1.33-25	2.27-27	3.41-27
	114.5		1.01-25	1.90-27				1.24-25	2.10-27	4.00-27
PLSA -27/-9	118.5		1.83-25	3.63-27				1.00-25	1.71-27	5.13-27
	122.5									0.504
	125.5									0.332

All calculations based on orientation of X and Y axes as shown in Fig. 1.

In this and all succeeding tables, the superscripts "A" and "B" refer to contributions from sources lying "above" and "below" the midplane, respectively.

*Read as 4.42×10^{-25} .

#Units are reactions/s/nucleus.

Table II. Calculated nickel reaction rate components at locations in the outer baffle*

Location	Axial level (cm)	A_{XY}	A_X	A_{XYZ}	B_{XYZ}	B_X	B_{XYZ}	B_X	B_{XYZ}	$A+B_{XYZ}$	$B_{XYZ}/A+B_{XYZ}$
O.B. -29/+2	106.5	1.69-25†	6.19-24	3.76-27	1.03-28‡	6.02-26	2.52-24	4.31-26	1.03-27‡	1.13-27‡	0.912
	110.5		6.91-27	1.89-28				5.99-26	1.43-27	1.62-27	0.983
114.5		1.26-26	3.64-28					7.13-26	1.70-27	2.04-27	0.832
118.5		2.30-26	6.28-28					7.83-26	1.87-27	2.50-27	0.749
122.5		4.22-26	1.15-27					7.83-26	1.87-27	3.02-27	0.619
125.5		6.80-26	1.86-27					7.32-26	1.75-27	3.61-27	0.485
128.5		1.14-25	3.11-27					6.00-26	1.43-27	4.54-27	0.315
131.5		1.58-25	4.31-27					5.26-26	1.26-27	5.57-27	0.226
134.5		2.00-25	5.46-27					3.72-26	8.89-28	6.35-27	0.140
137.5		2.17-25	5.92-27					2.68-26	6.40-28	6.56-27	0.098
141.5		2.18-25	5.95-27					1.62-26	3.87-28	6.36-27	0.061
145.5		2.00-25	5.46-27					9.45-27	2.26-28	5.69-27	0.040
149.5		1.68-25	4.59-27					5.47-27	1.31-28	4.72-27	0.028
153.5		1.19-25	3.25-27					3.14-27	7.50-29	3.33-27	0.023
O.B. -29/-2	114.5	1.61-25	6.19-24	1.26-26	3.28-28	5.75-26	2.52-24	7.13-26	1.63-27	1.36-27	0.833
	131.5		1.58-25	4.09-27				5.26-26	1.20-27	5.30-27	0.227
145.5		2.00-25	5.19-27					9.45-27	2.16-28	5.40-27	0.040
O.B. -29/-7	114.5	1.30-25	6.19-24	1.26-26	2.64-28	4.45-26	2.52-24	7.13-26	1.26-27	3.53-27	0.827
	131.5		1.58-25	3.30-27				5.26-26	9.31-28	4.23-27	0.220
145.5		2.00-25	4.18-27					9.45-27	1.67-28	4.35-27	0.039
O.B. -29/-12	114.5	7.55-26	6.19-24	1.26-26	1.54-28	3.28-26	2.52-24	7.13-26	9.30-28	1.08-27	0.858
	131.5		1.58-25	1.92-27				5.26-26	6.85-28	2.61-27	0.263
145.5		2.00-25	2.44-27					9.45-27	1.23-28	2.56-27	0.048
O.B. -27/-14	114.5	7.92-26	1.19-23	1.77-26	1.18-28	3.78-26	4.07-24	1.19-25	1.10-27	1.22-27	0.903
	131.5		3.63-25	2.29-27				8.56-26	7.96-28	3.08-27	0.258
145.5		4.02-25	2.68-27					1.37-26	1.28-28	2.80-27	0.046
O.B. -17/-14	114.5	1.55-25	2.44-23	2.82-26	1.79-28	1.07-25	1.62-23	5.24-25	3.48-27	3.66-27	0.951
	131.5		7.58-25	4.82-27				2.55-25	1.70-27	6.51-27	0.260
145.5		8.45-25	5.37-27					2.30-26	1.53-28	5.52-27	0.028
O.B. -17/-14	114.5	2.49-25	3.50-23	3.78-26	2.70-28	2.19-25	3.03-23	1.01-24	7.28-27	7.55-27	0.964
	131.5		1.10-24	7.85-27				4.77-25	3.45-27	1.13-26	0.305
145.5		1.20-24	8.57-27					3.62-26	2.48-28	8.82-27	0.028

*All calculations based on orientation of X and Y axes as shown in Fig. 1.

†Read as 1.69 $\times 10^{-25}$.

#Units are reactions/s/nucleus.

Table 12. Calculated nickel reaction rate components at locations in the core barrel

Location	Axial level (cm)	A R _{XY}	A R _{XZ}	A R _{YZ}	B R _{XY}	B R _{XZ}	B R _{YZ}	A+B R _{XYZ}	B+A R _{XYZ} /R _{XYZ}
C.B. 0°*	106.5	2.32-26†	9.26-25	1.47-27	3.71-29#	9.75-27	4.35-25	7.29-27	1.63-28#
(-37/+2)	110.5	2.54-27	6.39-29		9.08-27		2.03-28	2.67-28	0.816
114.5	4.24-27	1.07-28		1.06-26	2.37-28		3.43-28	0.761	
118.5	6.61-27	1.66-28		1.13-26	2.53-28		4.19-28	0.690	
122.5	9.81-27	2.47-28		1.12-26	2.51-28		4.97-28	0.505	
125.5	1.38-26	3.48-28		9.94-27	2.23-28		5.71-28	0.391	
128.5	1.75-26	4.41-28		9.22-27	2.06-28		6.48-28	0.319	
131.5	1.99-26	5.01-28		8.33-27	1.87-28		6.87-28	0.272	
134.5	2.29-26	5.75-28		7.32-27	1.64-28		7.39-28	0.222	
137.5	2.56-26	6.43-28		5.34-27	1.20-28		7.63-28	0.157	
141.5	2.60-26	6.53-28		3.75-27	8.39-29		7.37-28	0.114	
145.5	2.45-26	6.17-28		2.69-27	6.02-29		6.77-28	0.089	
149.5	2.15-26	5.41-28		1.73-27	3.87-29		5.80-28	0.067	
153.5	1.66-26	4.17-28		1.12-27	2.51-29		4.42-28	0.057	
C.B. 10°*	114.5	1.98-26	9.86-25	4.44-27	8.91-29	8.52-27	4.64-25	1.13-26	2.08-28
(-37/-5)	131.5	2.13-26	4.28-28		8.89-27		1.64-28	5.92-28	0.277
145.5	2.63-26	5.28-28		2.82-27	5.19-29		5.80-28	0.089	
C.B. 21°*	106.5	1.86-26	1.50-24	2.00-27	2.48-29	8.62-27	6.92-25	1.18-26	1.46-28
(-37/-12)	110.5	3.36-27	4.18-29		1.49-26		1.86-28	2.28-28	0.815
114.5	5.68-27	7.06-29		1.75-26	2.18-28		2.89-28	0.754	
118.5	9.44-27	1.17-28		1.87-26	2.33-28		3.50-28	0.663	
122.5	1.52-26	1.88-28		1.88-26	2.34-28		4.22-28	0.552	
125.5	2.10-26	2.61-28		1.67-26	2.08-28		4.69-28	0.441	
128.5	2.87-26	3.57-28		1.51-26	1.88-28		5.46-28	0.343	
131.5	3.34-26	4.15-28		1.36-26	1.69-28		5.84-28	0.288	
134.5	3.98-26	4.96-28		1.15-26	1.44-28		6.39-28	0.223	
137.5	4.36-26	5.43-28		8.15-27	1.02-28		6.44-28	0.157	
141.5	4.48-26	5.57-28		5.83-27	7.26-29		6.30-28	0.115	
145.5	4.20-26	5.22-28		3.85-27	4.79-29		5.79-28	0.084	
149.5	3.64-26	4.52-28		2.50-27	3.11-29		4.83-28	0.064	
153.5	2.75-26	3.42-28		1.50-27	1.87-29		3.60-28	0.052	

Table 12. Continued

Location	Axial level (cm)	A R _{XY}	A R _{XZ}	A R _{YZ}	B R _{XY}	B R _{XZ}	B R _{YZ}	B R _{XYZ}	B R _{XYZ}	A+B R _{XYZ}	B R _{XYZ} /A+B R _{XYZ}
C, B. 25°*	114.5	1.60-26	1.71-24	6.06-27	5.67-29	8.06-27	7.83-25	2.01-26	2.64-28	0.785	
	(-34/-15)	131.5	3.84-26	3.59-28	1.54-26	1.59-28	5.18-28	0.306			
	145.5	4.87-26	4.55-28	4.18-27	4.31-29	4.98-28	0.086				
C, B. 28°*	114.5	1.44-26	2.09-24	6.86-27	4.73-29	7.88-27	9.47-25	2.47-26	2.53-28	0.813	
	(-33/-17)	131.5	4.79-26	3.30-28	1.89-26	1.57-28	4.87-28	0.322			
	145.5	6.10-26	4.20-28	4.89-27	4.07-29	4.61-28	0.088				
C, B. 33°*	114.5	1.38-26	3.31-24	8.91-27	3.72-29	8.97-27	1.46-24	3.96-26	2.44-28	2.81-28	0.868
	(-31/-20)	131.5	7.93-26	3.31-28	2.97-26	1.83-28	5.14-28	0.356			
	145.5	1.02-25	4.24-28	6.54-27	4.03-29	4.64-28	0.087				
C, B. 40°*	114.5	1.25-26	8.78-24	1.54-26	2.18-29	9.38-27	3.26-24	9.38-26	2.70-28	2.92-28	0.925
	(-28/-24)	131.5	2.34-25	3.32-28	6.85-26	1.97-28	5.29-28	0.372			
	145.5	2.88-25	4.08-28	1.16-26	3.35-29	4.42-28	0.076				
C, B. 45°*	106.5	1.23-26	1.48-23	5.72-27	4.74-30	1.04-26	5.07-24	8.75-26	1.76-28	1.83-28	0.974
	(-26/-26)	110.5	1.05-26	8.68-30	1.24-25	2.54-28	2.63-28	0.967			
	114.5	1.95-26	1.61-29	1.51-25	3.08-28	3.24-28	0.950				
118.5	3.59-26	2.97-29	1.68-25	3.44-28	3.74-28	0.921					
	122.5	6.80-26	5.64-29	1.72-25	3.51-28	4.07-28	0.861				
	125.5	1.15-25	9.54-29	1.59-25	3.25-28	4.20-28	0.773				
128.5	2.16-25	1.79-28	1.29-25	2.63-28	4.43-28	0.595					
	131.5	4.45-25	3.69-28	1.06-25	2.16-28	5.85-28	0.369				
	134.5	5.38-25	4.46-28	7.01-26	1.43-28	5.89-28	0.243				
137.5	5.71-25	4.73-28	4.57-26	9.32-29	5.66-28	0.165					
	141.5	5.62-25	4.66-28	2.67-26	5.45-29	5.20-28	0.105				
	145.5	5.08-25	4.21-28	1.56-26	3.19-29	4.53-28	0.071				
149.5	4.23-25	3.50-28	8.84-27	1.81-29	3.68-28	0.049					
	153.5	3.17-25	2.63-28	5.02-27	1.03-29	2.73-28	0.038				

Table 12. Continued

Location	Axial level (cm)	A R _{XY}	A R _{XZ}	A R _{YZ}	B R _{XY}	B R _{XZ}	B R _{YZ}	A+B R _{XYZ}	B R _{XYZ}	A+B R _{XYZ}
C. B. 68°*	106.5	2.18-26	4.94-23	1.28-26	5.62-30	2.10-26	4.61-23	9.31-25	4.24-28	4.30-28
(-12/-35)	110.5	2.48-26	1.09-29		1.26-24	5.74-28	5.85-28	5.85-28	0.981	0.981
114.5	4.89-26	2.15-29		1.56-24	7.09-28	7.31-28			0.971	
118.5	9.81-26	4.32-29		1.79-24	8.15-28	8.58-28			0.950	
122.5	2.04-25	9.00-29		1.89-24	8.63-28	9.53-28			0.906	
125.5	3.66-25	1.61-28		1.85-24	8.44-28	1.01-27			0.840	
128.5	7.38-25	3.25-28		1.55-24	7.06-28	1.03-27			0.685	
131.5	1.60-24	7.04-28		7.10-25	3.24-28	1.03-27			0.315	
134.5	1.93-24	8.51-28		3.50-25	1.60-28	1.01-27			0.158	
137.5	2.00-24	8.83-28		1.94-25	8.85-29	9.72-28			0.091	
141.5	1.92-24	8.46-28		9.27-26	4.22-29	8.88-28			0.048	
145.5	1.70-24	7.47-28		4.59-26	2.09-29	7.68-28			0.027	
149.5	1.39-24	6.11-28		2.33-26	1.06-29	6.22-28			0.017	
153.5	1.03-24	4.56-28		1.20-26	5.45-30	4.61-28			0.012	
C. B. 89°*	106.5	2.80-26	6.28-23	1.65-26	7.36-30	2.73-26	6.12-23	1.25-24	5.54-28	5.61-28
(+2/-37)	110.5	3.22-26	1.43-29		1.68-24	7.48-28	7.62-28			0.981
114.5	6.35-26	2.83-29		2.08-24	9.25-28	9.53-28			0.970	
118.5	1.28-25	5.69-29		2.38-24	1.06-27	1.12-27			0.949	
122.5	2.65-25	1.18-28		2.51-24	1.12-27	1.24-27			0.905	
125.5	4.71-25	2.10-28		2.44-24	1.09-27	1.30-27			0.838	
128.5	9.50-25	4.23-28		2.04-24	9.07-28	1.33-27			0.682	
131.5	2.06-24	9.15-28		9.38-25	4.18-28	1.33-27			0.314	
134.5	2.47-24	1.10-27		4.64-25	2.06-28	1.31-27			0.158	
137.5	2.55-24	1.14-27		2.61-25	1.16-28	1.26-27			0.092	
141.5	2.43-24	1.08-27		1.25-25	5.58-29	1.14-27			0.049	
145.5	2.14-24	9.54-28		6.21-26	2.77-29	9.82-28			0.028	
149.5	1.75-24	7.77-28		3.14-26	1.40-29	7.91-28			0.018	
153.5	1.27-24	5.75-28		1.61-26	7.16-30	5.82-28			0.012	

Table 12. Continued

Location	Axial level (cm)	A _{RXY}	A _{RXZ}	A _{RXYZ}	B _{RXY}	B _{RXZ}	B _{RXYZ}	A+B _{RXYZ}	B _{RXYZ} /A+B _{RXYZ}
		A _{RXY}	A _{RXZ}	A _{RXYZ}	B _{RXY}	B _{RXZ}	B _{RXYZ}	A+B _{RXYZ}	B _{RXYZ} /A+B _{RXYZ}
C, B, 45°**	106.5	1.23-26	1.76-23	6.65-27	4.64-30	1.04-26	1.71-23	3.48-25	2.11-28
(-26/-26)	110.5	1.22-26	8.47-30	4.65-25	2.82-28	2.90-28	0.971	0.956	0.956
114.5	2.28-26	1.58-29	5.70-25	3.46-28	3.61-28	0.930	0.930	0.930	0.930
118.5	4.25-26	2.95-29	6.49-25	3.94-28	4.24-28	0.880	0.880	0.880	0.880
122.5	8.13-26	5.65-29	6.83-25	4.15-28	4.71-28	0.807	0.807	0.807	0.807
125.5	1.39-25	9.64-29	6.55-25	4.04-28	5.00-28	0.648	0.648	0.648	0.648
128.5	2.66-25	1.85-28	5.60-25	3.40-28	5.25-28	0.287	0.287	0.287	0.287
131.5	5.68-25	3.94-28	2.61-25	1.59-28	5.53-28	0.148	0.148	0.148	0.148
134.5	6.77-25	4.71-28	1.35-25	8.21-29	5.35-28	0.090	0.090	0.090	0.090
137.5	7.00-25	4.87-28	7.90-26	4.79-29	5.35-28	0.051	0.051	0.051	0.051
141.5	6.69-25	4.65-28	4.10-26	2.49-29	4.90-28	0.031	0.031	0.031	0.031
145.5	5.92-25	4.11-28	2.18-26	1.33-29	4.24-28	0.021	0.021	0.021	0.021
149.5	4.85-25	3.37-28	1.16-26	7.05-30	3.44-28	0.015	0.015	0.015	0.015
153.5	3.63-25	2.52-28	6.30-27	3.82-30	2.56-28				
C, B, 68°**	106.5	2.18-26	1.75-24	2.37-27	2.95-29	2.10-26	1.68-24	2.93-26	3.96-28
(-12/-35)	110.5	4.00-27	4.98-29	4.01-26	5.01-28	5.51-28	0.909	0.909	0.909
114.5	6.78-27	8.45-29	4.69-26	5.86-28	6.70-28	0.874	0.874	0.874	0.874
118.5	1.13-26	1.41-28	5.08-26	6.35-28	7.76-28	0.818	0.818	0.818	0.818
122.5	1.82-26	2.27-28	5.03-26	6.29-28	8.54-28	0.735	0.735	0.735	0.735
125.5	2.52-26	3.14-28	4.65-26	5.81-28	8.94-28	0.649	0.649	0.649	0.649
128.5	3.46-26	4.31-28	3.88-26	4.85-28	9.16-28	0.529	0.529	0.529	0.529
131.5	4.00-26	4.98-28	3.37-26	4.21-28	9.19-28	0.458	0.458	0.458	0.458
134.5	4.79-26	5.97-28	2.45-26	3.06-28	9.02-28	0.339	0.339	0.339	0.339
137.5	5.19-26	6.47-28	1.76-26	2.20-28	8.66-28	0.254	0.254	0.254	0.254
141.5	5.27-26	6.56-28	1.10-26	1.38-28	7.93-28	0.173	0.173	0.173	0.173
145.5	4.88-26	6.08-28	6.55-27	8.17-29	6.89-28	0.119	0.119	0.119	0.119
149.5	4.19-26	5.22-28	3.84-27	4.80-29	5.70-28	0.084	0.084	0.084	0.084
153.5	3.13-26	3.90-28	2.27-27	2.84-29	4.18-28	0.068	0.068	0.068	0.068

Table 12. Continued

Location	Axial level (cm)	Δ R_{XY}	Δ R_X	Δ R_{XZ}	Δ R_{XYZ}	B R_X	B R_{XZ}	$\frac{B}{\Delta}$ R_{XYZ}	B R_{XYZ}	$\Delta + B$ R_{XYZ}	B R_{XYZ}	$\Delta + B$ R_{XYZ}/R_{XYZ}
C, B, 89°**	106.5	2.80-26	1.08-24	1.74-27	4.52-29	2.73-26	1.03-24	1.78-26	4.70-28	5.15-28	0.912	
(+2/-37)	110.5			3.03-27	7.87-29			2.38-26	6.27-28	7.06-28	0.888	
114.5				5.08-27	1.32-28			2.74-26	7.22-28	8.54-28	0.845	
118.5				7.91-27	2.06-28			2.94-26	7.74-28	9.80-28	0.790	
122.5				1.17-26	3.04-28			2.94-26	7.76-28	1.08-27	0.719	
125.5				1.66-26	4.31-28			2.64-26	6.95-28	1.13-27	0.617	
128.5				2.10-26	5.47-28			2.30-26	6.06-28	1.15-27	0.526	
131.5				2.37-26	6.16-28			2.04-26	5.39-28	1.16-27	0.467	
134.5				2.72-26	7.07-28			1.61-26	4.25-28	1.13-27	0.375	
137.5				3.04-26	7.89-28			1.13-26	2.99-28	1.09-27	0.275	
141.5				3.04-26	7.91-28			7.67-27	2.02-28	9.93-28	0.204	
145.5				2.85-26	7.40-28			4.91-27	1.29-28	8.70-28	0.149	
149.5				2.48-26	6.45-28			2.92-27	7.69-29	7.22-28	0.106	
153.5				1.89-26	4.91-28			1.66-27	4.38-29	5.35-28	0.082	

*Calculations based on orientation of X and Y axes as shown in Fig. 1.

#Units are reactions/s/nucleus.

†Read as 2.32×10^{-26} .

**Calculations based on orientation of X and Y axes rotated 90° to that of Fig. 1.

Table 13. Calculated nickel reaction rate components for the supplementary locations

Location	Axial level (cm)	A R _{XY}	A R _{XZ}	B R _{XYZ}	B R _{XY}	B R _{XZ}	B R _{XYZ}	A+B R _{XYZ}	B R _{XYZ} /R _{XYZ}
3.3% Fuel	106.05	7.50-25†	2.64-23	7.77-27	2.20-28#	5.48-25	1.98-23	3.54-25	9.82-27#
21/+2*	110.15	1.51-26	4.27-28					5.14-25	1.42-26
	114.25	2.92-26	8.29-28					6.40-25	1.77-26
	118.35	5.70-26	1.62-27					7.47-25	2.07-26
	122.45	1.14-25	3.24-27					8.06-25	2.23-26
	125.55	2.03-25	5.76-27					7.99-25	2.22-26
	128.65	4.11-25	1.17-26					6.68-25	1.85-26
	131.75	8.43-25	2.39-26					2.88-25	7.99-27
	134.85	1.01-24	2.86-26					1.46-25	4.05-27
	137.95	1.05-24	2.98-26					8.42-26	2.33-27
	141.05	1.03-24	2.92-26					5.07-26	1.40-27
	145.15	9.27-25	2.63-26					2.64-26	7.31-28
	149.25	7.63-25	2.17-26					1.39-26	3.84-28
	153.35	5.62-25	1.60-26					7.25-27	2.01-28
3.3% Fuel	106.05	8.44-25	3.05-23	8.68-27	2.40-28	6.81-25	2.50-23	4.48-25	1.22-26
-19/+3*	110.15	1.68-26	4.64-28					6.55-25	1.78-26
	114.25	3.25-26	8.99-28					8.17-25	2.22-26
	118.35	6.47-26	1.79-27					9.52-25	2.59-26
	122.45	1.32-25	3.65-27					1.02-24	2.78-26
	125.55	2.36-25	6.53-27					1.00-24	2.74-26
	128.65	4.80-25	1.33-26					8.31-25	2.27-26
	131.75	9.73-25	2.69-26					3.77-25	1.03-26
	134.85	1.17-24	3.23-26					1.88-25	5.12-27
	137.95	1.21-24	3.36-26					1.06-25	2.89-27
	141.05	1.19-24	3.28-26					6.15-26	1.67-27
	145.15	1.06-24	2.95-26					3.04-26	8.29-28
	149.25	8.76-25	2.43-26					1.56-26	4.25-28
	153.35	6.45-25	1.79-26					8.15-27	2.22-28

Table 13. Continued

Location	Axial level (cm)	A R _{XY}	A R _{XZ}	A R _{YZ}	B R _{XY}	B R _{XZ}	B R _{YZ}	B R _{XYZ}	A+B R _{XYZ}	B R _{XYZ} /A+B R _{XYZ}
3.3% Fuel	106.05	6.90-25	2.44-23	7.36-27	2.08-28	4.41-25	1.62-23	2.87-25	7.82-27	8.03-27
-22/0*	110.15			1.42-26	4.00-28			4.16-25	1.13-26	1.17-26
114.25				2.71-26	7.67-28			5.18-25	1.41-26	0.946
118.35				5.27-26	1.49-27			6.02-25	1.64-26	0.916
122.45				1.04-25	2.95-27			6.48-25	1.77-26	0.857
125.55				1.86-25	5.27-27			6.40-25	1.74-26	0.768
128.65				3.77-25	1.07-26			5.34-25	1.46-26	0.53-26
131.75				7.76-25	2.20-26			2.42-25	6.61-27	2.86-26
134.85				9.26-25	2.62-26			1.28-25	3.50-27	2.97-26
137.95				9.66-25	2.73-26			7.51-26	2.05-27	2.94-26
141.05				9.48-25	2.68-26			4.60-26	1.26-27	2.81-26
145.15				8.56-25	2.42-26			2.43-26	6.63-28	2.49-26
149.25				7.06-25	2.00-26			1.30-26	3.54-28	2.04-26
153.35				5.20-25	1.47-26			6.89-27	1.88-28	1.49-26
Water Gap	106.5	5.27-26	2.09-24	2.40-27	6.05-29	2.12-26	9.47-25	1.61-26	3.60-28	4.21-28
-33/+2	110.5			4.11-27	1.04-28			2.11-26	4.72-28	5.76-28
114.5				6.86-27	1.73-28			2.47-26	5.53-28	7.26-28
118.5				1.16-26	2.92-28			2.66-26	5.95-28	8.87-28
122.5				1.96-26	4.94-28			2.68-26	5.99-28	1.09-27
125.5				2.78-26	7.01-28			2.41-26	5.38-28	1.24-27
128.5				4.02-26	1.02-27			2.12-26	4.74-28	1.49-27
131.5				4.79-26	1.21-27			1.89-26	4.22-28	1.63-27
134.5				5.87-26	1.48-27			1.54-26	3.45-28	1.83-27
137.5				6.40-26	1.62-27			1.09-26	2.44-28	1.86-27
141.5				6.55-26	1.65-27			7.45-27	1.67-28	1.82-27
145.5				6.10-26	1.54-27			4.89-27	1.09-28	1.65-27
149.5				5.20-26	1.31-27			3.05-27	6.83-29	1.38-27
153.5				3.86-26	9.76-28			1.84-27	4.11-29	1.02-27

Table 13. Continued

Location	Axial level (cm)	A R _{XY}	A R _{XZ}	B R _{XY}	B R _{XZ}	B R _{YZ}	A+B R _{XYZ}	B R _{XYZ}	A+B R _{XYZ}	B R _{XYZ}	A+B R _{XYZ}
3.3% Fuel	106.05	7.57-25	6.28-23	1.54-26	1.86-28	7.44-25	6.12-23	1.15-24	1.40-26	1.42-26	0.987
+2/+23*	110.15			3.04-26	3.67-28			1.65-24	2.00-26	2.04-26	0.982
114.25				6.10-26	7.35-28			2.05-24	2.49-26	2.56-26	0.971
118.35				1.25-25	1.50-27			2.37-24	2.88-26	3.03-26	0.950
122.45				2.63-25	3.17-27			2.51-24	3.04-26	3.36-26	0.906
125.55				4.76-25	5.74-27			2.44-24	2.96-26	3.53-26	0.838
128.65				1.00-24	1.21-26			1.99-24	2.41-26	3.62-26	0.666
131.75				2.11-24	2.54-26			8.84-25	1.07-26	3.51-26	0.296
134.85				2.49-24	3.00-26			4.35-25	5.28-27	3.53-26	0.150
137.95				2.55-24	3.07-26			2.41-25	2.92-27	3.36-26	0.087
141.05				2.45-24	2.95-26			1.37-25	1.66-27	3.12-26	0.053
145.15				2.18-24	2.62-26			6.62-26	8.04-28	2.70-26	0.030
149.25				1.77-24	2.13-26			3.28-26	3.99-28	2.17-26	0.018
153.35				1.32-24	1.59-26			1.65-26	2.01-28	1.67-26	0.012
3.3% Fuel	106.05	7.57-25	2.46-23	7.30-27	2.25-28	7.44-25	2.38-23	4.46-25	1.40-26	1.42-26	0.984
+2/+23**	110.15			1.39-26	4.27-28			6.40-25	2.00-26	2.04-26	0.979
114.25				2.65-26	8.18-28			7.92-25	2.48-26	2.56-26	0.969
118.35				5.19-26	1.60-27			9.14-25	2.86-26	3.02-26	0.947
122.45				1.05-25	3.23-27			9.65-25	3.02-26	3.34-26	0.904
125.55				1.88-25	5.78-27			9.40-25	2.94-26	3.52-26	0.835
128.65				3.89-25	1.29-26			7.70-25	2.41-26	3.61-26	0.668
131.75				8.20-25	2.53-26			3.41-25	1.07-26	3.60-26	0.297
134.85				9.65-25	2.97-26			1.69-25	5.30-27	3.50-26	0.151
137.95				9.87-25	3.04-26			9.48-26	2.97-27	3.34-26	0.088
141.05				9.50-25	2.93-26			5.52-26	1.73-27	3.10-26	0.056
145.15				8.46-25	2.61-26			2.79-26	8.74-28	2.70-26	0.032
149.25				6.89-25	2.12-26			1.45-26	4.53-28	2.17-26	0.021
153.35				5.16-25	1.59-26			7.57-27	2.37-28	1.61-26	0.015

Table 13. Continued

Location	Axial level (cm)	A	A	A	B	B	B	A+B
		R _{XY}	R _X	R _{XZ}	R _{XYZ}	R _{XY}	R _X	R _{XZ}
PLSA	131.05	3.40-25	1.19-23	3.22-25	9.21-27	1.00-25	4.07-24	8.79-26
-27/+2*	134.15			4.13-25	1.18-26			2.16-27
	137.25			4.46-25	1.28-26			1.33-26
	141.35			4.44-25	1.27-26			0.113
	145.45			4.02-25	1.15-26			0.072
	149.55			3.35-25	9.59-27			0.044
	153.65			2.44-25	6.99-27			0.029
						8.01-27	1.97-28	9.79-27
						4.47-27	1.10-28	7.10-27
								0.015
PLSA	131.05	5.06-25	1.74-23	4.95-25	1.44-26	1.65-25	6.48-24	1.40-25
-25/+3*	134.15			6.35-25	1.84-26			8.90-26
	137.25			6.79-25	1.97-26			5.63-26
	141.35			6.70-25	1.95-26			3.18-26
	145.45			6.04-25	1.76-26			1.76-26
	149.55			4.99-25	1.45-26			9.74-27
	153.65			3.62-25	1.05-26			5.35-27
								1.36-28
								1.06-26
								0.013
PLSA	131.05	6.41-25	2.22-23	6.38-25	1.84-26	3.18-25	1.19-23	2.38-25
-23/+2*	134.15			8.20-25	2.37-26			1.29-25
	137.25			8.74-25	2.52-26			7.56-26
	141.35			8.59-25	2.48-26			3.98-26
	145.45			7.71-25	2.23-26			2.13-26
	149.55			6.35-25	1.83-26			1.14-26
	153.65			4.56-25	1.32-26			6.14-27

*Calculations based on orientation of X and Y axes as shown in Fig. 1.

^tRead as 7.50 x 10⁻²⁵.

#Units are reactions/nucleus.

**Calculations based on orientation of X and Y axes rotated 90° to that in Fig. 1.

Table 14. Calculated indium reaction rate components for all locations

Location	Axial level	A_{RXY}	A_{RXZ}	A_{RXYZ}	B_{RXY}	B_{RXZ}	B_{RXYZ}	B_{RXYZ}/R_{XYZ}	$A+B_{RXYZ}$	$B_{RXYZ}/A+B_{RXYZ}$
O.B. -29/+2*	106.5 110.5 114.5 118.5 122.5 125.5 128.5 131.5 134.5 137.5 141.5 145.5 149.5 153.5	3.49-25† 1.26-23 1.34-26 2.51-26 4.69-26 8.78-26 1.42-25 2.33-25 3.26-25 4.10-25 4.46-25 4.49-25 4.10-25 3.43-25 2.40-25	1.92-28# 3.69-28 6.94-28 1.30-27 2.43-27 3.91-27 6.45-27 9.03-27 1.13-26 1.23-26 1.24-26 1.24-26 1.13-26 9.47-27 6.64-27	1.28-25 5.12-24 3.69-28 1.47-25 1.62-25 1.61-25 1.51-25 1.24-25 1.04-25 7.30-26 5.15-26 3.04-26 1.73-26 9.74-27 5.36-27	8.63-26 1.22-25 3.68-27 4.05-27 4.05-27 3.78-27 3.12-27 2.61-27 1.83-27 1.29-27 7.63-28 4.34-28 2.44-28 1.34-28	2.17-27# 3.06-27 4.37-27 5.35-27 6.48-27 7.69-27 9.57-27 1.16-26 1.31-26 1.36-26 1.32-26 1.17-26 9.71-27 6.77-27	2.36-27# 3.43-27 4.37-27 5.35-27 6.48-27 7.69-27 9.57-27 1.16-26 1.31-26 1.36-26 0.058 0.037 0.025 0.020	0.919 0.892 0.841 0.757 0.625 0.492 0.326 0.224 0.139 0.095 0.058 0.037 0.025 0.020	0.870 0.832 0.771 0.676 0.551 0.435 0.318 0.251 0.179 0.125 0.085 0.060 0.043 0.034	
Water Gap -33/+2*	106.5 110.5 114.5 118.5 122.5 125.5 128.5 131.5 134.5 137.5 141.5 145.5 149.5 153.5	9.47-26 3.68-24 6.61-27 1.15-26 1.99-26 3.42-26 4.90-26 7.10-26 8.62-26 1.05-25 1.15-25 1.18-25 1.09-25 9.26-26 6.84-26	9.48-29 3.74-26 1.70-28 2.95-28 5.13-28 8.80-28 1.27-27 1.83-27 2.22-27 2.72-27 2.96-27 3.03-27 2.81-27 2.39-27 1.76-27	3.68-24 1.63-24 4.32-26 4.68-26 4.70-26 4.26-26 3.72-26 3.24-26 2.58-26 1.83-26 1.22-26 7.75-27 4.70-27 2.73-27	2.76-26 3.67-26 9.92-28 1.07-27 1.08-27 9.77-28 8.54-28 7.44-28 5.92-28 4.21-28 2.80-28 1.78-28 1.08-28 6.26-29	6.33-28 8.42-28 1.29-27 1.58-27 1.96-27 2.25-27 2.68-27 2.96-27 3.31-27 3.38-27 3.31-27 2.99-27 2.50-27 1.82-27	7.28-28 1.01-27 0.771 0.676 0.551 0.435 0.318 0.251 0.179 0.125 0.085 0.060 0.043 0.034			

Table 14. Continued

Location	Axial level (cm)	A R _{XY}	A R _{XZ}	A R _{YZ}	B R _{XY}	B R _{XZ}	B R _{YZ}	A+B R _{XYZ}	B R _{XYZ}	A+B R _{XYZ}
C. B. 0°*	106.5	4.57-26	1.90-24	2.65-27	6.37-29	1.88-26	8.69-25	1.43-26	3.08-28	3.72-28
(-37/+2)	110.5	4.75-27	1.14-28			1.84-26	3.97-28	5.11-28	0.777	0.829
114.5	8.13-27	1.96-28			2.15-26	4.64-28	6.60-28	0.703		
118.5	1.31-26	3.16-28			2.30-26	4.97-28	8.13-28	0.611		
122.5	2.01-26	4.84-28			2.29-26	4.95-28	9.79-28	0.506		
125.5	2.80-26	6.75-28			2.06-26	4.45-28	1.12-27	0.397		
128.5	3.61-26	8.69-28			1.88-26	4.07-28	1.28-27	0.319		
131.5	4.20-26	1.01-27			1.67-26	3.61-28	1.37-27	0.263		
134.5	4.86-26	1.17-27			1.42-26	3.07-28	1.48-27	0.208		
137.5	5.38-26	1.29-27			1.05-26	2.26-28	1.52-27	0.149		
141.5	5.48-26	1.32-27			7.29-27	1.57-28	1.48-27	0.106		
145.5	5.16-26	1.24-27			4.97-27	1.07-28	1.35-27	0.079		
149.5	4.47-26	1.08-27			3.14-27	6.78-29	1.15-27	0.059		
153.5	3.35-26	8.07-28			1.90-27	4.10-29	8.48-28	0.048		
C. B. 28°*	106.5	3.17-26	3.68-24	3.68-27	3.17-29	1.67-26	1.63-24	2.76-26	2.82-28	3.14-28
(-33/-17)	110.5	6.61-27	5.69-29			3.67-26	3.75-28	4.32-28	0.868	0.899
114.5	1.15-26	9.87-29			4.32-26	4.42-28	5.41-28	0.817		
118.5	1.99-26	1.72-28			4.68-26	4.78-28	6.50-28	0.735		
122.5	3.42-26	2.94-28			4.70-26	4.80-28	7.74-28	0.620		
125.5	4.90-26	4.22-28			4.26-26	4.35-28	8.57-28	0.508		
128.5	7.10-26	6.11-28			3.72-26	3.80-28	9.91-28	0.383		
131.5	8.62-26	7.42-28			3.24-26	3.32-28	1.07-27	0.309		
134.5	1.05-25	9.08-28			2.58-26	2.64-28	1.17-27	0.225		
137.5	1.15-25	9.89-28			1.83-26	1.87-28	1.18-27	0.159		
141.5	1.18-25	1.01-27			1.22-26	1.25-28	1.14-27	0.110		
145.5	1.09-25	9.39-28			7.75-27	7.93-29	1.02-27	0.078		
149.5	9.26-26	7.97-28			4.70-27	4.80-29	8.45-28	0.057		
153.5	6.84-26	5.89-28			2.73-27	2.79-29	6.17-28	0.045		

Table 14. Continued

Axial level Location	A R _{XY}	A R _X	A R _{XZ}	B R _{XYZ}	B R _X	B R _{XZ}	B R _{XYZ}	A+B R _{XYZ}	B R _{XYZ} /R _{XYZ}
C, B, 89°*	106.5	5.46-26	1.11-22	2.55-26	1.25-29	5.33-26	1.09-22	2.20-24	1.09-27
(+2/-37)	110.5			5.16-26	2.54-29		2.98-24	1.46-27	1.49-27
114.5				1.05-25	5.16-29		3.69-24	1.81-27	1.86-27
118.5				2.17-25	1.07-28		4.23-24	2.08-27	2.19-27
122.5				4.61-25	2.27-28		4.46-24	2.19-27	2.42-27
125.5				8.33-25	4.09-28		4.34-24	2.13-27	2.54-27
128.5				1.68-24	8.26-28		3.62-24	1.78-27	2.61-27
131.5				3.66-24	1.80-27		1.66-24	8.16-28	2.62-27
134.5				4.40-24	2.16-27		8.21-25	4.03-28	2.56-27
137.5				4.54-24	2.23-27		4.54-25	2.23-28	2.45-27
141.5				4.33-24	2.13-27		2.13-25	1.05-28	2.24-27
145.5				3.81-24	1.87-27		1.03-25	5.06-29	1.92-27
149.5				3.10-24	1.52-27		5.04-26	2.48-29	1.54-27
153.5				2.28-24	1.12-27		2.48-26	1.22-29	1.13-27
C, B, 89°**	106.5	5.46-26	2.29-24	3.18-27	7.57-29	5.33-26	2.21-24	3.76-26	9.82-28
(+2/-37)	110.5			5.72-27	1.36-28		5.14-26	1.24-27	1.38-27
114.5				9.87-27	2.35-28		5.98-26	1.44-27	1.68-27
118.5				1.61-26	3.83-28		6.45-26	1.56-27	1.94-27
122.5				2.47-26	5.88-28		6.43-26	1.55-27	2.14-27
125.5				3.46-26	8.23-28		5.84-26	1.41-27	2.23-27
128.5				4.48-26	1.07-27		5.05-26	1.22-27	2.29-27
131.5				5.20-26	1.24-27		4.37-26	1.05-27	2.29-27
134.5				6.02-26	1.43-27		3.36-26	8.11-28	2.24-27
137.5				6.63-26	1.58-27		2.40-26	5.79-28	2.16-27
141.5				6.67-26	1.59-27		1.56-26	3.77-28	1.97-27
145.5				6.21-26	1.48-27		9.57-27	2.31-28	1.71-27
149.5				5.36-26	1.28-27		5.52-27	1.33-28	1.41-27
153.5				3.97-26	9.46-28		3.04-27	7.34-29	1.02-27

Table 14. Continued

Location	Axial level (cm)	A R _{XY}	A R _{XZ}	B R _{XY}	B R _{XZ}	B R _{XYZ}	B R _{XYZ}	A+B R _{XYZ}	B R _{XYZ}	A+B R _{XYZ}
		A R _{XY}	A R _{XZ}	B R _{XY}	B R _{XZ}	B R _{XYZ}	B R _{XYZ}	A+B R _{XYZ}	B R _{XYZ}	A+B R _{XYZ}
C, B, 33°*	106.5	2.85-26	6.26-24	4.75-27	2.16-29	1.78-26	2.71-24	4.57-26	3.01-28	3.23-28
(-31/-20)	110.5			8.84-27	4.02-29			6.30-26	4.14-28	4.54-28
114.5				1.61-26	7.31-29			7.47-26	4.91-28	5.64-28
118.5				2.90-26	1.32-28			8.15-26	5.36-28	6.68-28
122.5				5.19-26	2.36-28			8.14-26	5.35-28	7.71-28
125.5				7.95-26	3.62-28			7.52-26	4.94-28	8.56-28
128.5				1.20-25	5.48-28			6.37-26	4.19-28	9.67-28
131.5				1.54-25	6.98-28			5.47-26	3.59-28	1.06-27
134.5				1.90-25	8.63-28			4.09-26	2.68-28	1.13-27
137.5				2.08-25	9.48-28			2.93-26	1.92-28	1.14-27
141.5				2.12-25	9.63-28			1.85-26	1.21-28	1.08-27
145.5				1.95-25	8.87-28			1.10-26	7.25-29	9.60-28
149.5				1.64-25	7.44-28			6.35-27	4.17-29	7.86-28
153.5				1.17-25	5.31-28			3.57-27	2.35-29	5.55-28
C, E, 10°*	114.5	4.04-26	1.90-24	8.12-27	1.73-28	1.70-26	8.67-25	2.15-26	4.22-28	5.95-28
(-37/-5)	131.5			4.19-26	8.95-28			1.67-26	3.27-28	1.22-27
145.5				5.14-26	1.10-27			4.97-27	9.75-29	1.20-27
C, B, 21°*	114.5	3.97-26	2.46-24	9.20-27	1.48-28	1.80-26	1.11-24	2.83-26	4.59-28	6.01-28
(-37/-12)	131.5			5.58-26	8.99-28			2.18-26	3.52-28	1.25-27
145.5				6.95-26	1.12-27			5.93-27	9.60-29	1.22-27
C, B, 25°*	114.5	3.48-26	2.96-24	1.00-26	1.18-28	1.72-26	1.33-24	3.45-26	4.47-28	5.65-28
(-34/-15)	131.5			6.81-26	8.00-28			2.61-26	3.38-28	1.14-27
145.5				8.57-26	1.01-27			6.59-27	8.53-29	1.10-27
C, B, 40°*	114.5	2.40-26	1.72-23	2.96-26	4.14-29	1.80-26	6.52-24	1.89-25	5.22-28	5.63-28
(-28/-24)	131.5			4.65-25	6.51-28			1.32-25	3.65-28	1.02-27
145.5				5.68-25	7.95-28			2.07-26	5.71-29	8.52-28

Table 14. Continued

Location	Axial level (cm)	$A_{R_{XY}}$	$A_{R_{XZ}}$	$A_{R_{YZ}}$	$B_{R_{XY}}$	B_{R_X}	$B_{R_{XZ}}$	$B_{R_{YZ}}$	$A+B_{R_{XYZ}}$	$B_{R_{XYZ}}/R_{XYZ}$
C.B. $45^\circ*$ $(-26/-2)$	114.5	2.36-26	2.70-23	3.50-26	3.05-27	1.97-26	9.62-24	2.89-25	5.92-28	6.23-28
	131.5			8.19-25	7.15-28			1.92-25	3.95-28	1.11-27
	145.5			9.33-25	8.14-28			2.58-26	5.30-29	8.67-28
C.B. $45^\circ**$ $(-26/-26)$	114.5	2.36-26	3.23-23	3.86-26	2.82-29	1.97-26	3.13-23	1.05-24	6.62-28	6.90-28
	131.5			1.04-24	7.62-28			4.80-25	3.03-28	1.07-27
	145.5			1.09-24	7.95-28			3.71-26	2.34-29	8.18-28
68°* $(-12/-35)$	114.5	4.64-26	9.06-23	8.32-26	4.26-29	4.48-26	8.47-23	2.87-24	1.52-27	0.973
	131.5			2.94-24	1.50-27			1.31-24	6.93-28	2.19-27
	145.5			3.12-24	1.60-27			7.84-26	4.15-29	1.64-27
68°** $(-12/-35)$	114.5	4.64-26	3.04-24	1.11-26	1.70-28	4.48-26	2.93-24	8.28-26	1.27-27	1.44-27
	131.5			7.09-26	1.08-27			5.86-26	8.97-28	1.98-27
	145.5			8.60-26	1.31-27			1.08-26	1.65-28	1.48-27
I.B. $-1/+2*$	131.5	9.39-25	1.29-22	4.22-24	3.07-26	9.01-25	1.26-22	1.96-24	1.40-26	4.47-26
I.B. $-1/-1*$	131.5	1.14-24	1.29-22	4.22-24	3.73-26	1.09-24	1.26-22	1.96-24	1.70-26	5.43-26
										0.313

*Calculations based on orientation of X and Y axes as shown in Fig. 1.

†Read as 3.49×10^{-25} .

#Units are reactions/s/nucleus.

**Calculations based on orientation of X and Y axes rotated 90° to that in Fig. 1.

Table 15. Calculated aluminum reaction rate components

Location	Axial level	A R _{XY}	A R _{XZ}	A R _{XYZ}	B R _{XY}	B R _{XZ}	B R _{XYZ}	A+B R _{XYZ}	B R _{XYZ}	A+B R _{XYZ}
O.B. -29/+2*	114.5	1.06-27†	4.06-26	1.09-28	2.85-30#	4.19-28	1.86-26	5.02-28	1.13-29#	1.42-29#
	131.5	9.85-28	2.57-29		3.89-28		8.76-30	3.45-29		0.799
	145.5	1.26-27	3.29-29		8.40-29	1.89-30	3.48-29		0.254	0.054
Water Gap -33/+2*	114.5	4.05-28	1.70-26	6.77-29	1.61-30	1.83-28	8.71-27	2.16-28	4.54-30	6.15-30
	131.5	3.69-28	8.79-30		1.70-28		3.57-30	1.24-29		0.738
	145.5	4.72-28	1.12-29		5.04-29	1.06-30	1.23-29		0.289	0.086
C.B. 0°*	114.5	1.84-28	8.44-27	4.54-29	9.90-31	8.66-29	4.47-27	1.03-28	2.00-30	2.99-30
	131.5	1.72-28	3.75-30		8.30-29	1.61-30		5.36-30		0.669
	145.5	2.11-28	4.60-30		3.03-29	5.87-31		5.19-30		0.300
C.B. 10°*	114.5	1.57-28	8.44-27	4.54-29	8.45-31	7.58-29	4.47-27	1.03-28	1.75-30	2.60-30
	131.5	1.72-28	3.20-30		8.30-29	1.41-30		4.61-30		0.306
	145.5	2.11-28	3.93-30		3.03-29	5.14-31		4.44-30		0.113
C.B. 21°*	114.5	1.41-28	1.23-26	5.61-29	6.43-31	7.36-29	6.40-27	1.53-28	1.76-30	2.40-30
	131.5	2.58-28	2.96-30		1.22-28		1.40-30	4.36-30		0.732
	145.5	3.24-28	3.71-30		4.00-29	4.60-31		4.17-30		0.321
C.B. 25°*	114.5	1.22-28	1.44-26	6.08-29	5.15-31	6.93-29	7.46-27	1.83-28	1.70-30	2.22-30
	131.5	3.08-28	2.61-30		1.44-28		1.34-30	3.95-30		0.339
	145.5	3.91-28	3.31-30		4.42-29	4.11-31		3.72-30		0.110
C.B. 28°*	114.5	1.09-28	1.70-26	6.77-29	4.34-31	6.67-29	8.71-27	2.16-28	1.65-30	2.08-30
	131.5	3.69-28	2.37-30		1.70-28		1.30-30	3.67-30		0.792
	145.5	4.72-28	3.03-30		5.04-29	3.86-31		3.42-30		0.354
C.B. 33°*	114.5	1.14-28	2.42-26	8.32-29	3.92-31	8.08-29	1.21-26	3.13-28	2.09-30	2.48-30
	131.5	5.52-28	2.60-30		2.45-28	1.64-30		4.2-30		0.842
	145.5	7.10-28	3.34-30		6.33-29	4.23-31		3.76-30		0.387

Table 15. Continued

Location	Axial level	A _{R_{XY}}	A _{R_{XZ}}	A _{R_{YZ}}	B _{R_{XY}}	B _{R_{XZ}}	B _{R_{YZ}}	A+B _{R_{XYZ}}	B+A+B _{R_{XYZ}}
C, B, 40°*	114.5	1.13-28	5.98-26	1.34-28	2.53-31	8.64-29	2.37-26	6.50-28	2.37-30
	131.5			1.45-27	2.74-30			4.99-28	1.82-30
	145.5			1.80-27	3.40-30			1.03-28	3.75-31
C, B, 45°**	114.5	1.11-28	1.15-25	1.95-28	1.88-31	9.58-29	1.11-25	3.61-27	3.12-30
	131.5			3.57-27	3.45-30			1.74-27	1.50-30
	145.5			3.75-27	3.62-30			1.86-28	1.61-31
C, B, 68°**	114.5	1.63-28	1.48-26	6.67-29	7.35-31	1.56-28	1.42-26	3.79-28	4.16-30
	131.5			3.21-28	3.54-30			2.83-28	3.11-30
	145.5			3.95-28	4.35-30			6.40-29	7.03-31
C, B, 89°**	114.5	2.22-28	1.01-26	5.46-29	1.20-30	2.16-28	9.63-27	2.42-28	5.43-30
	131.5			2.09-28	4.59-30			1.89-28	4.24-30
	145.5			2.52-28	5.54-30			5.25-29	1.18-30
I, B, -1/+2*	131.5	2.75-27	4.03-25	1.28-26	8.73-29	2.63-27	3.91-25	6.16-27	4.14-29
I, B, -1/-1*	131.5	3.23-27	4.03-25	1.28-26	1.03-28	3.10-27	3.91-25	6.16-27	4.88-29
									1.29-28
									0.322
									0.321

*Calculations based on orientation of X and Y axes as shown in Fig. 1.

#Units are reactions/s/nucleus.

†Read as 1.06×10^{-27} .

**Calculations based on orientation of X and Y axes rotated 90° to that in Fig. 1.

4. COMPARISON OF THE MEASUREMENTS AND CALCULATIONS

The values of the measured nickel reaction rates may be reconstructed from the fission equivalent fluxes which were presented in Tables 2 through 4 by multiplying by the value used for the nickel cross section averaged over the ^{235}U fission spectrum, which was 108.5 mb (Footnote d). The calculated reaction rates presented in the next-to-last column of Tables 10 through 13 must be multiplied by the source normalization factor 8.845×10^8 (see Section 2.4). The resulting absolute comparisons are shown in Tables 16 through 18 for the early run and Table 19 for the supplementary run.

Similarly, values of the measured indium reaction rates may be reconstructed by multiplying the fission equivalent fluxes presented in Table 5 by the value used by Mol for the indium cross section averaged over the ^{235}U fission spectrum, which was 190.3 mb (Footnote d). Again, the calculated indium reaction rates presented in the next-to-last column of Table 14 must be multiplied by the factor 8.845×10^8 . The resulting absolute comparisons are shown in Table 20.

Values of the measured aluminum reaction rates may be similarly obtained by multiplying the entries in Table 6 by the Mol value for the aluminum fission averaged cross section, which was 0.706 mb (Footnote e). Renormalizing the calculated reaction rates in Table 15 as before leads to the comparisons shown in Table 21.

Table 16. Absolute comparisons of the nickel reaction rates in the inner baffle and PLSA in units of reactions per second per nucleus at 100% power (early run)

Axial level (cm)	Location	R _C	R _E	R _C /R _E	Location	R _C	R _E	R _C /R _E
114.5	I.B. -1/+2	1.31-16*	1.34-16	0.98	I.B. -1/-1	1.58-16	1.61-16	0.98
		1.86-16	1.91-16	0.97		2.24-16	2.28-15	0.98
		1.37-16	1.36-16	1.01		1.66-16	1.66-16	1.00
106.5	PLSA -27/+2	1.65-17	1.80-17	0.92	PLSA -25/+2	2.71-17	2.95-17	0.92
110.5		2.38-17	2.51-17	0.95		3.94-17	4.19-17	0.94
114.5		3.03-17	3.22-17	0.94		4.98-17	5.34-17	0.93
118.5		3.70-17	3.87-17	0.96		6.01-17	6.43-17	0.93
122.5		4.45-17	4.66-17	0.95		7.09-17	7.58-17	0.94
125.5		5.25-17	5.52-17	0.95		8.18-17	8.70-17	0.94
128.5		6.81-17	7.36-17	0.93		1.03-16	1.12-16	0.92
106.5	PLSA -23/+2	5.26-17	5.58-17	0.94	PLSA -27/-9	1.13-17	1.24-17	0.91
110.5		7.54-17	7.81-17	0.97		1.64-17	1.61-17	1.02
114.5		9.55-17	9.93-17	0.96		2.08-17	1.95-17	1.07
118.5		1.14-16	1.19-16	0.96		2.52-17	2.41-17	1.05
112.5		1.31-16	1.38-16	0.95		3.02-17	2.88-17	1.05
125.5		1.46-16	1.53-16	0.95		3.54-17	3.49-17	1.01
128.5		1.68-16	1.77-16	0.95		4.54-17	4.86-17	0.93

*Read as 1.31×10^{-16} .

Table 17. Absolute comparisons of the nickel reaction rates in the outer baffle
in units of reactions per second per nucleus at 100% power (early run)

Axial level (cm)	Location	R_C	R_E	R_C/R_E	Axial level (cm)	Location	R_C	R_E	R_C/R_E
106.5	O.B. -29/+2	9.99-18*	1.07-17	0.93	114.5	O.B. -29/-2	1.73-17	1.78-17	0.97
110.5		1.43-17	1.48-17	0.97	131.5		4.69-17	5.06-17	0.93
114.5		1.80-17	1.91-17	0.94	145.5		4.78-17	5.06-17	0.94
118.5		2.21-17	2.30-17	0.96					
122.5		2.67-17	2.81-17	0.95	114.5	O.B. -29/-7	1.35-17	1.48-17	0.91
125.5		3.19-17	3.36-17	0.95	131.5		3.74-17	4.15-17	0.90
128.5		4.02-17	4.23-17	0.95	145.5		3.85-17	4.12-17	0.93
131.5		4.93-17	5.45-17	0.90					
134.5		5.62-17	6.07-17	0.93	114.5	O.B. -29/-12	9.55-18	9.81-18	0.97
137.5		5.80-17	6.25-17	0.93	131.5		2.31-17	2.41-17	0.96
141.5		5.61-17	6.04-17	0.93	145.5		2.26-17	2.36-17	0.96
145.5		5.03-17	5.39-17	0.93					
149.5		4.17-17	4.42-17	0.94	114.5	O.B. -27/-14	1.08-17	1.15-17	0.94
153.5		2.95-17	3.17-17	0.93	131.5		2.72-17	2.61-17	1.04
					145.5		2.48-17	2.42-17	1.02
					114.	O.B. -22/-14	3.24-17	3.36-17	0.96
					131.5		5.76-17	5.66-17	1.02
					145.5		4.88-17	4.73-17	1.03
					114.5	O.B. -17/-14	6.68-17	6.80-17	0.98
					131.5		9.99-17	1.01-16	0.99
					145.5		7.80-17	7.75-i7	1.01

*Read as 9.99×10^{-18} .

Table 18. Absolute comparisons of the nickel reaction rates in the core barrel
in units of reactions per second per nucleus at 100% power (early run)

Axial level (cm)	Location	R_C	R_E	R_C/RE	Location	R_C	R_E	R_C/RE
106.5	C.B. 0° (-37/+2)	1.77-18*†	1.85-18	0.96	C.B. 21° (-35/-12)	1.51-18†	1.54-18	0.98
110.5		2.36-18	2.42-18	0.98		2.02-18	2.10-18	0.96
114.5	3.03-18	3.08-18	0.98			2.56-18	2.60-18	0.98
118.5	3.71-18	3.92-18	0.95			3.10-18	3.23-18	0.96
122.5	4.40-18	4.78-18	0.92			3.73-18	3.88-18	0.96
125.5	5.05-18	5.38-18	0.94			4.15-18	4.41-18	0.94
128.5	5.73-18	6.04-18	0.95			4.83-18	4.95-18	0.98
131.5	6.08-18	6.64-18	0.92			5.17-18	5.48-18	0.94
134.5	6.54-18	7.03-18	0.93			5.65-18	5.90-18	0.96
137.5	6.75-18	7.28-18	0.93			5.70-18	6.02-13	0.95
141.5	6.52-18	7.02-18	0.93			5.57-18	5.83-18	0.96
145.5	5.99-18	6.40-18	0.94			5.04-18	5.21-18	0.97
149.5	5.13-18	5.38-18	0.95			4.27-18	4.41-18	0.97
153.5	3.91-18	4.10-18	0.95			3.18-18	3.35-18	0.95
106.5	C.B. 45° (-26/-26)	1.62-18†	1.91-18	0.85	C.B. 45° (-26/-26)	1.91-18#	1.91-18	1.00
110.5		2.33-18	2.45-18	0.95		2.57-18	2.45-18	1.05
114.5	2.87-18	2.99-18	0.96			3.19-18	2.99-18	1.07
118.5	3.31-18	3.45-18	0.96			3.75-18	3.45-18	1.09
122.5	3.60-18	3.85-18	0.94			4.17-18	3.85-18	1.08
125.5	3.71-18	4.08-18	0.91			4.42-18	4.08-18	1.08
128.5	3.92-18	4.19-18	0.94			4.64-18	4.19-18	1.11
131.5	5.17-18	4.21-18	1.23			4.89-18	4.21-18	1.16
134.5	5.21-18	4.19-18	1.24			4.89-18	4.19-18	1.17
137.5	5.01-18	4.15-18	1.21			4.73-18	4.15-18	1.14
141.5	4.60-18	3.82-18	1.20			4.33-18	3.82-18	1.13
145.5	4.01-18	3.37-18	1.19			3.75-18	3.37-18	1.11
149.5	3.25-18	2.77-18	1.17			3.04-18	2.77-18	1.10
153.5	2.41-18	2.15-18	1.12			2.26-18	2.15-18	1.05

Table 18. Continued

Axial level (cm)	Location	R _C	R _E	R _{C/RE}	Location	R _C	R _E	R _{C/RE}
106.5	C.B. 68° (-12/-35)	3.50-18#	0.94	C.B. 89° (+2/-37)	4.56-18#	4.71-18	0.97	
110.5	4.87-18	5.07-18	0.96		6.24-18	6.34-18	0.98	
114.5	5.93-18	6.23-18	0.95		7.55-18	7.72-18	0.98	
118.5	6.86-18	7.09-18	0.97		8.67-18	8.94-18	0.97	
122.5	7.55-18	7.73-18	0.98		9.55-18	9.74-18	0.98	
125.5	7.91-18	8.15-18	0.97		9.99-18	1.02-17	0.98	
128.5	8.10-18	8.19-18	0.99		1.02-17	1.04-17	0.98	
131.5	8.13-18	8.37-18	0.97		1.03-17	1.05-17	0.98	
134.5	7.98-18	8.17-18	0.98		9.99-18	1.03-17	0.97	
137.5	7.66-18	7.89-18	0.97		9.64-18	9.87-18	0.98	
141.5	7.01-18	7.24-18	0.97		8.78-18	8.95-18	0.98	
145.5	6.09-18	6.23-18	0.98		7.70-18	7.82-18	0.98	
149.5	5.04-18	5.09-18	0.99		6.39-18	6.33-18	1.01	
153.5	3.70-18	3.76-18	0.98		4.73-18	4.71-18	1.00	
106.5	C.B. 68° (-12/-35)	3.75-18†	3.73-18	1.01 (+2/-37)	C.B. 89° (+2/-37)	4.96-18†	4.71-18	1.05
110.5	5.17-18	5.07-18	1.02		6.74-18	6.34-18	1.06	
114.5	6.47-18	6.23-18	1.05		8.43-18	7.72-18	1.09	
118.5	7.59-18	7.09-18	1.07		9.91-18	8.94-18	1.11	
122.5	8.43-18	7.73-18	1.09		1.10-17	9.74-18	1.13	
125.5	8.89-18	8.15-18	1.09		1.15-17	1.02-17	1.13	
128.5	9.11-18	8.19-18	1.11		1.18-17	1.04-17	1.13	
131.5	9.11-18	8.37-18	1.09		1.18-17	1.05-17	1.12	
134.5	8.93-18	8.17-18	1.09		1.16-17	1.03-17	1.13	
137.5	8.60-18	7.89-18	1.09		1.11-17	9.87-18	1.12	
141.5	7.85-18	7.24-18	1.08		1.01-17	8.95-18	1.13	
145.5	6.79-18	6.23-18	1.09		8.69-18	7.82-18	1.11	
149.5	5.50-18	5.09-18	1.08		7.00-18	6.33-18	1.11	
153.5	4.08-18	3.76-18	1.09		5.15-18	4.71-18	1.09	

Table 18. Continued

Axial level (cm)	Location	R_C	R_E	R_C/R_E	Location	R_C	R_E	R_C/R_E
114.5	C.B. 10°	2.63-18†	2.71-18	0.87	C.B. 25° (-34/-15)	2.34-18†	2.38-18	0.98
	(-37/-5)	5.24-18	5.68-18	0.92				
	131.5	5.13-18	5.49-18	0.93				
145.5	C.B. 28°	2.24-18†	2.30-18	0.97	C.B. 33° (-31/-20)	2.49-18†	3.14-18	0.79
	(-33/-17)	4.31-18	4.30-18	1.00				
	131.5	4.08-18	4.00-18	1.02				
145.5	C.B. 40°	2.58-18†	2.76-18	0.93	C.B. 45° (-28/-24)	4.55-18	4.88-18	0.93
	(-28/-24)	4.68-18	4.10-18	1.14				
	131.5	3.91-18	3.33-18	1.17				

*Read as 1.77×10^{-18} .

†Calculations based on orientation of X and Y axes as shown in Fig. 1.

#Calculations based on orientation of X and Y axes rotated 90° to that of Fig. 1.

Table 19. Absolute comparisons of the nickel reaction rates in units of reactions per second per nucleus at 100% power (supplementary run)

Axial level	Location	R_C	R_E	R_C/R_E	Axial level (cm)	Location	R_C	R_E	R_C/R_E
106.5	Water Gap	3.72-18*†	4.05-18	0.92	106.05	3.3% Fuel 1	7.10-17†	8.31-17	0.85
110.5	-33/+2	5.09-18	5.45-18	0.93	110.15	-22/+0	1.03-16	1.15-16	0.90
114.5		6.42-18	6.91-18	0.93	114.25		1.32-16	1.46-16	0.90
118.5		7.85-18	8.34-18	0.94	118.35		1.58-16	1.76-16	0.90
122.5		9.64-18	1.04-17	0.93	122.45		1.83-16	2.04-16	0.90
125.5		1.10-17	1.22-17	0.90	125.55		2.01-16	2.24-16	0.90
128.5		1.32-17	1.44-17	0.92	128.65		2.24-16	2.47-16	0.91
131.5		1.44-17	1.64-17	0.88	131.75		2.53-16	2.74-16	0.92
134.5		1.62-17	1.79-17	0.91	134.85		2.63-16	2.85-16	0.92
137.5		1.65-17	1.82-17	0.91	137.95		2.60-16	2.84-16	0.92
141.5		1.61-17	1.78-17	0.90	141.05		2.49-16	2.71-16	0.92
145.5		1.46-17	1.57-17	0.93	145.15		2.20-16	2.40-16	0.92
149.5		1.22-17	1.31-17	0.93	149.25		1.80-16	1.98-16	0.91
153.5		9.02-18	9.39-18	0.96	153.35		1.32-16	1.49-16	0.89
106.05	3.3% Fuel 1	8.85-17†	1.01-16	0.88	106.05	3.3% Fuel 1	1.10-16†	1.24-16	0.89
110.15	-21/+2	1.29-16	1.39-16	0.93	110.15	-19/+3	1.62-16	1.72-16	0.94
114.25		1.64-16	1.78-16	0.92	114.25		2.04-16	2.19-16	0.93
118.35		1.97-16	2.15-16	0.92	118.35		2.45-16	2.63-16	0.93
122.45		2.26-16	2.47-16	0.91	122.45		2.79-16	3.01-16	0.93
125.55		2.48-16	2.71-16	0.92	125.55		3.00-16	3.24-16	0.93
128.65		2.67-16	2.91-16	0.92	128.65		3.18-16	3.43-16	0.93
131.75		2.80-16	3.10-16	0.90	131.75		3.29-16	3.54-16	0.93
134.85		2.89-16	3.17-16	0.91	134.85		3.31-16	3.57-16	0.93
137.95		2.84-16	3.10-16	0.92	137.95		3.23-16	3.49-16	0.93
141.05		2.71-16	2.98-16	0.91	141.05		3.05-16	3.30-16	0.92
145.15		2.39-16	2.61-16	0.92	145.15		2.68-16	2.91-16	0.92
149.25		1.95-16	2.13-16	0.92	149.25		2.18-16	2.38-16	0.92
153.35		1.43-16	1.60-16	0.89	153.35		1.60-16	1.79-16	0.89

Table 19. Continued

Axial level (cm)	Location	R_C	R_E	R_C/R_E	Axial level (cm)	Location	R_C	R_E	R_C/R_E
106.05	3.3% Fuel	1.26-16†	1.39-16	0.91	106.05	3.3% Fuel	1	1.26-16#	1.39-16
110.15	+2/+23	1.80-16	1.92-16	0.94	110.15	+2/+23	1	1.80-16	1.92-16
114.25		2.26-16	2.40-16	0.94	114.25		2	2.27-16	2.40-16
118.35		2.68-16	2.83-16	0.95	118.35		2	2.67-16	2.83-16
122.45		2.97-16	3.14-16	0.95	122.45		2	2.95-16	3.14-16
125.55		3.12-16	3.30-16	0.95	125.55		3	3.11-16	3.30-15
128.65		3.20-16	3.39-16	0.94	128.65		3	3.19-16	3.39-16
131.75		3.19-16	3.38-16	0.94	131.75		3	3.18-16	3.38-16
134.85		3.12-16	3.31-16	0.94	134.85		3	3.10-16	3.31-16
137.95		2.97-16	3.14-16	0.95	137.95		2	2.95-16	3.14-16
141.05		2.76-16	2.94-16	0.94	141.05		2	2.74-16	2.94-16
145.15		2.39-16	2.53-16	0.94	145.15		2	2.39-16	2.53-16
149.25		1.92-16	2.05-16	0.94	149.25		1	1.92-16	2.05-16
153.35		1.48-16	1.52-16	0.97	153.35		1	1.42-16	1.52-16
131.05	PLSA	-27/+2	1.01-16†	1.18-16	0.86	131.05	PLSA	-25/+3	1.59-16†
134.15		1.18-16	1.34-16	0.88	134.15		1	1.83-16	1.75-16
137.25		1.22-16	1.39-16	0.88	137.25		1	1.87-16	2.00-16
141.35		1.18-16	1.33-16	0.89	141.35		1	1.80-16	2.00-16
145.45		1.04-15	1.20-16	0.87	145.45		1	1.59-16	1.77-16
149.55		8.66-17	9.90-17	0.87	149.55		1	1.30-16	1.47-16
153.65		6.28-17	7.62-17	0.82	153.65		9	9.38-17	1.12-16
131.05	PLSA	-23/+2	2.19-16†	2.47-16	0.89				0.91
134.15		2.40-16	2.63-16	0.91			2	2.00-16	0.92
137.25		2.41-16	2.65-16	0.91			2	2.06-16	0.91
141.35		2.29-16	2.51-16	0.91			1	2.00-16	0.90
145.45		2.03-16	2.20-16	0.92			1	1.59-16	0.90
149.55		1.65-16	1.80-16	0.92			1	1.30-16	0.88
153.65		1.19-16	1.36-16	0.88			9	9.38-17	0.84

*Read as 3.72 x 10⁻¹⁸.

†Calculations based on orientation of X and Y axes as shown in Fig. 1.

#Calculations based on orientation of X and Y axes rotated 90° to that of Fig. 1.

Table 20. Absolute comparisons of the indium reaction rates in units of reactions per second per nucleus at 100% power

Axial level (cm)	Location	R_C	R_E	R_C/R_E	Axial level (cm)	Location	R_C	R_E	R_C/R_E
106.5	O.B. -29/+2	2.09-17†	0.92	106.5	Water Gap	6.44-18†	7.17-18	0.90	
110.5	3.03-17	3.23-17	0.94	110.5	-33/+2	8.93-18	9.87-18	0.90	
114.5	3.87-17	4.15-17	0.93	114.5		1.14-17	1.26-17	0.90	
118.5	4.73-17	5.06-17	0.93	118.5		1.40-17	1.57-17	0.89	
122.5	5.73-17	6.20-17	0.92	122.5		1.73-17	1.90-17	0.91	
125.5	6.80-17	7.37-17	0.92	125.5		1.99-17	2.26-17	0.88	
128.5	8.46-17	9.25-17	0.91	128.5		2.37-17	2.67-17	0.89	
131.5	1.03-16	1.16-16	0.89	131.5		2.57-17	2.96-17	0.87	
134.5	1.16-16	1.32-16	0.88	134.5		2.93-17	3.28-17	0.89	
137.5	1.20-16	1.37-16	0.88	137.5		2.99-17	3.49-17	0.86	
141.5	1.17-16	1.31-16	0.89	141.5		2.93-17	3.40-17	0.86	
145.5	1.03-16	1.18-16	0.87	145.5		2.64-17	3.04-17	0.87	
149.5	8.59-17	9.63-17	0.89	149.5		2.21-17	2.56-17	0.86	
153.5	5.99-17	6.88-17	0.87	153.5		1.61-17	1.91-17	0.84	
106.5	C.B. 0° (-37/+2)	3.29-18†	0.91	106.5	C.B. 28° (-33/-17)	2.78-18†	3.08-18	0.90	
110.5	4.52-18	5.01-18	0.90	110.5		3.82-18	4.28-18	0.89	
114.5	5.84-18	6.40-18	0.91	114.5		4.79-18	5.41-18	0.89	
118.5	7.19-18	7.93-18	0.91	118.5		5.75-18	6.51-18	0.88	
122.5	8.66-18	9.67-18	0.90	122.5		6.85-18	7.68-18	0.89	
125.5	9.91-18	1.12-17	0.88	125.5		7.58-18	8.47-18	0.89	
128.5	1.13-17	1.26-17	0.90	128.5		8.77-18	9.39-18	0.93	
131.5	1.21-17	1.43-17	0.85	131.5		9.46-18	1.01-17	0.94	
134.5	1.31-17	1.50-17	0.87	134.5		1.03-17	1.06-17	0.97	
137.5	1.34-17	1.56-17	0.86	137.5		1.04-17	1.09-17	0.95	
141.5	1.31-17	1.51-17	0.87	141.5		1.01-17	1.04-17	0.97	
145.5	1.19-17	1.37-17	0.87	145.5		9.02-18	9.31-18	0.97	
149.5	1.02-17	1.16-17	0.88	149.5		7.47-18	8.23-18	0.91	
153.5	7.50-18	8.64-18	0.87	153.5		5.46-18	5.79-18	0.94	

Table 20. Continued

Axial level (cm)	Location	R_C	R_E	R_C/R_E	Axial level (cm)	Location	R_C	R_E	R_C/R_E
106.5	C.B. 89° (+2/-37)	9.64-18†	1.06-17	0.91	106.5	C.B. 89° (+2/-37)	8.69-18#	1.06-17	0.82
110.5		1.32-17	1.37-17	0.96	110.5		1.22-17	1.27-17	0.89
114.5		1.65-17	1.64-17	1.01	114.5		1.49-17	1.64-17	0.91
118.5		1.94-17	1.90-17	1.02	118.5		1.72-17	1.90-17	0.91
122.5		2.14-17	2.10-17	1.02	122.5		1.89-17	2.10-17	0.90
125.5		2.25-17	2.17-17	1.04	125.5		1.97-17	2.17-17	0.91
128.5		2.31-17	2.22-17	1.04	128.5		2.03-17	2.22-17	0.91
131.5		2.32-17	2.21-17	1.05	131.5		2.03-17	2.21-17	0.92
134.5		2.26-17	2.20-17	1.03	134.5		1.98-17	2.20-17	0.90
137.5		2.17-17	2.11-17	1.03	137.5		1.91-17	2.11-17	0.91
141.5		1.98-17	1.91-17	1.04	141.5		1.74-17	1.91-17	0.91
145.5		1.70-17	1.65-17	1.03	145.5		1.51-17	1.65-17	0.92
149.5		1.36-17	1.45-17	0.94	149.5		1.25-17	1.45-17	0.86
153.5		1.00-17	9.61-18	1.04	153.5		9.02-18	9.61-18	0.94
106.5	C.B. 33° (-31/-20)	2.86-18†	3.23-18	0.89	114.5	C.B. 10° (-37/-5)	5.26-18†	5.93-18	0.89
110.5		4.02-18	4.42-18	0.91	131.5		1.08-17	1.26-17	0.86
114.5		4.99-18	5.49-18	0.91	145.5		1.06-17	1.24-17	0.85
118.5		5.91-18	6.56-18	0.90					
122.5		6.81-18	7.53-18	0.91	114.5	C.B. 21° (-35/-12)	5.37-18†	5.98-18	0.90
125.5		7.57-18	8.25-18	0.92	131.5		1.11-17	1.24-17	0.90
128.5		8.55-18	8.90-18	0.96	145.5		1.08-17	1.20-17	0.90
131.5		9.38-18	9.43-18	0.99					
134.5		9.99-18	9.67-18	1.03	114.5	C.B. 25° (-34/-15)	5.00-18†	5.35-18	0.90
137.5		1.01-17	9.75-18	1.04	131.5		1.01-17	1.10-17	0.92
141.5		9.55-18	9.25-18	1.03	145.5		9.73-18	1.03-17	0.94
145.5		8.49-18	8.36-18	1.02					
149.5		6.95-18	7.32-18	0.95					
153.5		4.91-18	5.14-18	0.96					

Table 20. Continued

Axial level (cm)	Location	R_C	R_E	R_C/R_E	Axial level (cm)	Location	R_C	R_E	R_C/R_E
114.5	C.B. 45°	5.51-18†	6.06-18	0.91	114.5	C.B. 45°	6.10-18#	6.06-18	1.01
131.5	(-26/-26)	9.82-18	8.76-18	1.12	131.5	(-26/-26)	9.46-18	8.76-18	1.08
145.5	7.67-18	6.95-18	1.10	145.5		7.24-18	6.95-18	1.04	
114.5	C.B. 68°	1.38-17†	1.39-17	0.99	114.5	C.B. 68°	1.27-17#	1.39-17	0.91
131.5	(-12/-35)	1.94-17	1.90-17	1.02	131.5	(-12/-35)	1.75-17	1.90-17	0.92
145.5	1.45-17	1.42-17	1.02	145.5		1.31-17	1.42-17	0.92	
114.5	C.B. 40°	4.98-18†	5.57-18	0.89	131.5	I.B. -1/+2	3.95-16†	4.28-16	0.92
131.5	(-28/-24)	9.02-18	8.48-18	1.06					
145.5	7.54-18	6.87-18	1.10	131.5	I.B. -1/-1	4.80-16†	5.16-16	0.93	

*Read as 2.09×10^{-17} .

†Calculations based on orientation of X and Y axes as shown in Fig. 1.

#Calculations based on orientation of X and Y axes rotated 90° to that of Fig. 1.

Table 21. Absolute comparisons of the aluminum reaction rates in units of reactions per second per nucleus at 100% power

Axial level (cm)	Location	R _C	R _E	R _C /R _E	Axial level (cm)	Location	R _C	R _E	R _C /R _E
114.5	O.B. -29/+2	1.26-19*	1.31-19	0.96	114.5	Water Gap	5.44-20†	5.91-20	0.92
131.5		3.05-19	3.38-19	0.90	131.5	-33/+2	1.10-19	1.32-19	0.83
145.5		3.08-19	3.36-19	0.92	145.5		1.09-19	1.26-19	0.87
114.5	C.B. 0°	2.64-20†	2.90-20	0.91	114.5	C.B. 10°	2.30-20†	2.26-20	1.02
131.5		4.74-20	5.41-20	0.88	131.5		4.08-20	4.46-20	0.91
145.5		4.59-20	5.13-20	0.89	145.5		3.93-20	4.25-20	0.92
114.5	C.B. 21°	2.12-20†	2.23-20	0.95	114.5	C.B. 25°	1.96-20†	2.15-20	0.91
131.5		3.86-20	4.25-20	0.91	131.5		3.49-20	3.76-20	0.93
145.5		3.69-20	4.03-20	0.92	145.5		3.29-20	3.39-20	0.97
114.5	C.B. 28°	1.84-20†	1.94-20	0.95	114.5	C.B. 33°	2.19-20†	2.24-20	0.98
135.5		3.25-20	3.51-20	0.93	131.5		3.75-20	3.64-20	1.03
145.5		3.02-20	3.06-20	0.99	145.5		3.33-20	3.07-20	1.08
114.5	C.B. 40°	2.32-20†	2.60-20	0.89	114.5	C.B. 45°	2.93-20#	2.69-20	1.09
131.5		4.03-20	3.87-20	1.04	131.5		4.38-20	3.91-20	1.12
145.5		3.34-20	3.02-20	1.11	145.5		3.34-20	2.99-20	1.12
114.5	C.B. 68°	4.33-20#	4.81-20	0.90	114.5	C.B. 89°	5.86-20#	5.75-20	0.87
131.5		5.88-20	6.29-20	0.93	131.5		7.81-20	8.49-20	0.92
145.5		4.47-20	4.62-20	0.97	145.5		5.94-20	6.25-20	0.95
131.5	I.B. -1/+2	1.14-18†	1.10-18	1.04	131.5	I.B. -1/-1	1.34-18†	1.36-18	0.99

*Read as 1.26×10^{-19} .

†Calculations based on orientation of X and Y axes as shown in Fig. 1.

#Calculations based on orientation of X and Y axes rotated 90° to that of Fig. 1.

5. DISCUSSION AND CONCLUSIONS

An inspection of the comparisons presented in Tables 16 through 18 shows a pleasing agreement, generally lying within about 8% and usually much closer. There is evidence of a slightly (3% to 4%) low bias in the calculations.

Turning next to the comparisons in Table 19 which correspond to the supplementary nickel run, it is apparent that the agreement is a little poorer than for the earlier run with the bias increasing to the vicinity of 9%. This seems to suggest the presence of a small inconsistency in the power levels of the two nickel runs of the order of 5%. The indium dosimeters were exposed during several different runs, and the comparisons in Table 20 also indicate an average bias comparable with that of the later nickel run, although the indium comparisons are somewhat more erratic. (Observe, for example, the C/E values for locations lying above versus below the midplane at 0° and 28° in the core barrel.) The results for the aluminum dosimeters also suggest a calculational bias in the vicinity of those for both the indium and the later nickel runs.

The general agreement among all four series of results, although adequate, may be improved even more by comparing equivalent fission fluxes rather than reaction rates. The use of these fluxes removes some of the dependence of the calculated reaction rates on the dosimeter cross sections, and the resulting comparisons tend to become better measures of the accuracy of the transport calculations themselves, which is the primary goal of the VENUS-3 program. The nickel, indium, and aluminum cross

Table 22. Comparison between measured and calculated ^{235}U and ^{252}Cf fission spectrum averaged cross sections for nickel, indium, and aluminum

Reaction	χ_{82}			χ_{25}		
	Calculated (mb)	Measured (mb)	C/E	Calculated (mb)	Measured (mb)	C/E
$^{58}\text{Ni}(\text{n},\text{p})$	114	118	0.966	105.4	108.5	0.971
$^{115}\text{In}(\text{n},\text{n}')$	183	196	0.934	180.3	190.3	0.948
$^{27}\text{Al}(\text{n},\alpha)$	0.984	1.006	0.978	0.670	0.706	0.949

sections in the ELXSIR library all have values averaged over several fission spectra that are slightly lower than the more accurate measured values (see Table 22). In particular, the ^{235}U fission flux comparisons for nickel would result in C/E values 3% higher for the supplementary run (3.5% higher for the earlier run since a measured value of 109 mb was used by ORNL to reconstruct these measured reaction rates), 5.5% higher for the indium, and 5.4% higher for aluminum compared to the corresponding reaction rate comparisons appearing in Tables 16 through 21. This results in virtually perfect agreement for the early nickel run fission flux comparisons, a bias of about 5% low for the calculations of the supplementary nickel results, and biases of also about 5% low for both the indium and aluminum results.

The validity of the flux synthesis approximation without recourse to any superposition procedure involving separate source component treatment is clearly demonstrated by the comparisons at the inner baffle in Tables 16, 20, and 21, and at the (+2/+23) location in Table 19, where there is excellent agreement throughout the complete range of axial locations. There is also a similar agreement at the 68° and 89° locations in the core barrel when the more accurate 90° axis orientation is used in the calculations. Although the calculations actually performed treated the two source components separately because multiple locations were being analyzed simultaneously, it is clear that this was not necessary for the above locations because of the existing symmetry in the source geometry of the nearby pins. It should also be observed that in the case of the +2/+23 location, which is positioned near the +Y axis at a fuel pin far from the PLSA, the calculations using each of the two orientations produce essentially identical results (see Table 13). This is probably because of the near-isotropy of the source and flux in the neighborhood of the pin.

Success in the introduction of a source decomposition and superposition technique and combining it with the flux synthesis procedure is demonstrated by the axial comparisons at the 0° , 10° , 21° , 25° , and 28° locations in the core barrel as well as the four PLSA locations, the water gap, and all seven locations in the outer baffle. The axial profiles at these locations are influenced by the PLSA and are asymmetric, as contrasted with the nearly perfect symmetry of the profiles located well inside the core and in the vicinity of the 68° and 89° core barrel locations. There is evidence of the onset of a possible breakdown of the assumptions leading to Eqs. (8) through (15) near the extreme top and bottom locations in some of these asymmetrical axial traverses, with the calculations generally underpredicting the measurements. A legitimate conclusion deduced from the comparisons near 0° and 90° is that, at least for VENUS-3, Eqs. (8) through (14) are as accurate in the treatment of the PLSA-affected regions as Eqs. (4) through (7) are in the treatment of the unaffected ones.

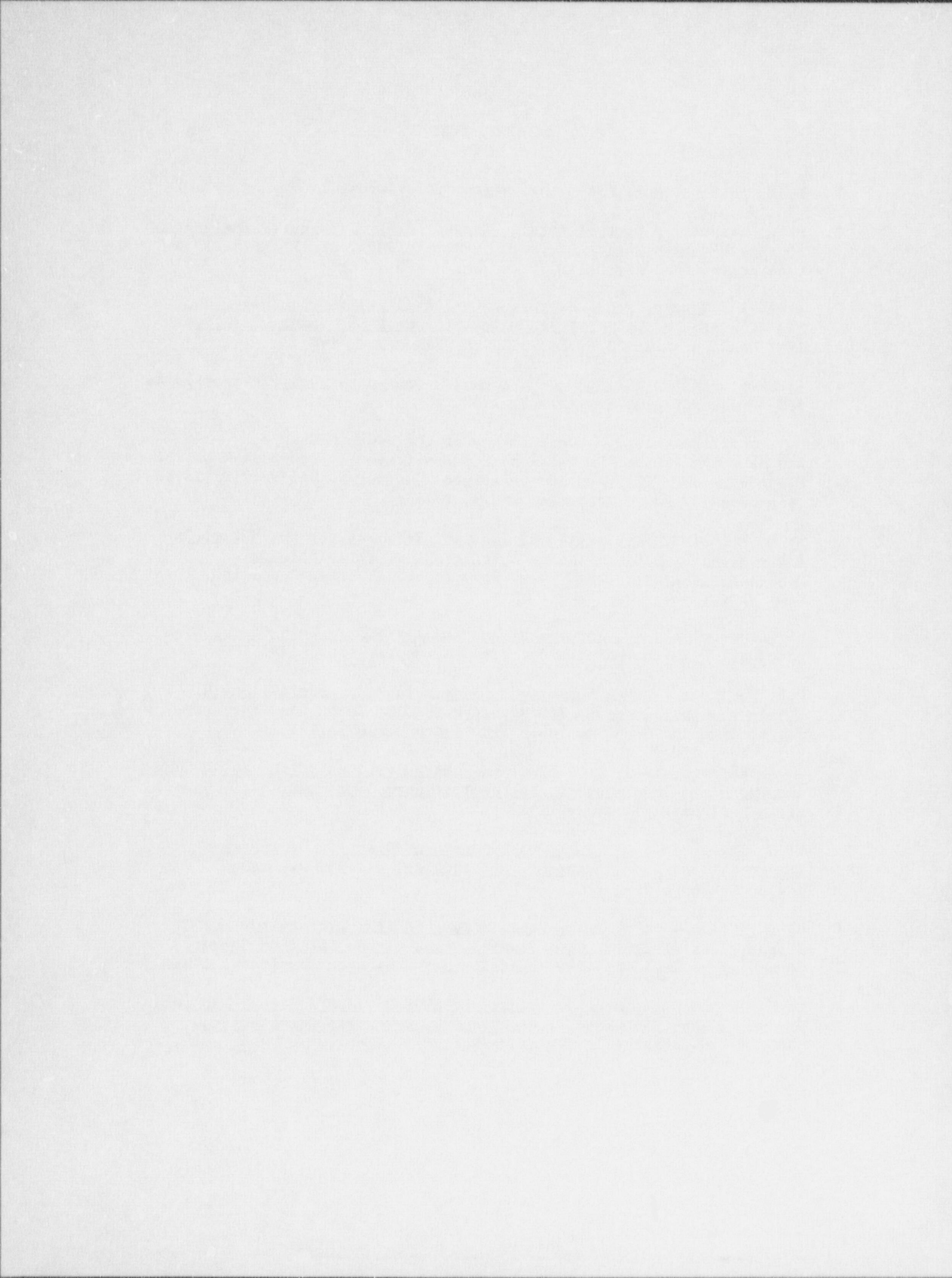
It is only at the three remaining locations, i.e., in the vicinity of 45° in the core barrel (i.e., 33° , 40° , and 45°), that any significant error is incurred using the superposition-synthesis procedure, and presumably this error could be greatly reduced by reorienting the X and Y axes in Eqs. (9)

through (15) to lie at 45° to the original directions indicated in Fig. 1. This would result in summing the source components along different directions and redefining the X-Z and X geometries. The error using the 0° and 90° orientations in the results at 33° , 40° , and 45° is still not large, being at most in the vicinity of 20% (see Table 18). The tendency of these calculations is to overpredict the component lying above the midplane (see Tables 18, 20, and 21), whereas the use of the 0° axis orientation in the calculation of the 68° and 89° fluxes tends to overestimate both the upper and lower components about equally (again, see Tables 18 and 20).

The conclusion that the method provides acceptable accuracy when applied to VENUS-3 does not necessarily imply that comparable accuracies should be realized when applied to PWRs. The differences in geometry, for example in the thickness of the PLSA, are considerable, being 6.3 cm for VENUS-3 as compared to around 20 cm for a typical PWR. This results in a larger differential attenuation between the PLSA and the fuel assemblies than was indicated for VENUS-3 in Table 8, thus possibly compromising the accuracy of the simplified geometries used in the X-Y and X calculations. Other geometrical differences involve the greater importance of the uncollided component in the VENUS-3 configuration, the truncation of the PLSA to less than half-core height in PWRs, and the more complicated effects occurring at the greater penetrations and into the cavities of PWRs produced by using PLSAs at only selected azimuths. Still, the accuracy of the proposed calculational technique when applied to VENUS-3 is encouraging, and bodes well for future PWR applications.

6. REFERENCES

1. R. E. Maerker, Nucl. Sci. Eng. 96(4), 263, August 1987.
2. R. E. Maerker, Report of Foreign Travel of R. E. Maerker, Engineering Physics and Mathematics Division, ORNL/FTR-2484, Oak Ridge National Laboratory, February 2, 1987.
3. A. Fabry, Results from Meetings at Mol Relative to the Design and Planning of the VENUS-3 PLSA Engineering Mock-Up, January 12-15, 1987, Reaktorfysika 33/87-04, SCK/CEN, January 2, 1987.
4. A. Fabry, VENUS-3 PLSA Conceptual Design Considerations, Reaktorfysika 380/87-02, SCK/CEN, February 2, 1987.
5. M. L. Williams et al., "Calculation of the Neutron Source Distribution in the VENUS PWR Mockup Experiment," Proceedings of the Fifth ASTM-EURATOM Symposium on Reactor Dosimetry, Volume 2, 711-718, Geesthacht, F.R.G., September 24-28, 1984.
6. M. L. Williams, Compilation of Contract Research for the Materials Engineering Branch, Division of Engineering, FY 1988 Annual Contractors Report, NUREG-0975, Vol. 7, U.S. Nuclear Regulatory Commission, 1989.
7. L. Leenders, LWR-PVS Benchmark Experiment VENUS-3, Core Description and Qualification, FCP/VEN/01, SCK/CEN, September 1, 1988.
8. H.B. Robinson Fluence Reduction Analysis for the Partial-Length Shield Assembly Concept, TEC Report R-83-030, Technology for Energy Corporation and Carolina Power and Light Company, 1983.
9. W. A. Rhoades and R. L. Childs, An Updated Version of the DOT 4 One- and Two-Dimensional Neutron/Photon Transport Code, ORNL-5851, Oak Ridge National Laboratory, 1982.
10. W. W. Engle, Jr., ANISN, A One-Dimensional Discrete Ordinates Transport Code with Anisotropic Scattering, K-1693, Oak Ridge National Laboratory, 1967.
11. M. L. Williams et al., The ELXSIR Cross-Section Library for LWR Pressure Vessel Irradiation Studies: Part of the LEPRICON Computer Code System, EPRI NP-3654, Electric Power Research Institute, 1984.
12. C. Y. Fu and D. M. Hetrick, Update of ENDF/B-V Mod-3 Iron: Neutron-Producing Reaction Cross Sections and Energy-Angle Correlations, ORNL/TM-9964, ENDF-341, Oak Ridge National Laboratory, 1986.



APPENDIX

Table A.1. Calculated neptunium reaction rate components and resulting equivalent fluxes*

Location	Axial level	A _{RXY}	A _{R_XZ}	A _{R_{XY}Z}	B _{R_{XY}}	B _{R_X}	B _{R_{XYZ}}	A+B _{R_{XYZ}}	B _{R_{XYZ}} /A+B _{R_{XYZ}}	Φ_{XYZ}
O. B. -29/+2	106.5	3.26-24†	1.17-22	6.37-26	1.77-27	1.18-24	4.81-23	7.97-25	1.95-26	2.13-26
	110.5		1.02-25	2.84-27		1.14-24		2.80-26	3.08-26	0.906
	114.5		2.38-25	6.63-27		1.38-24		3.39-26	4.05-26	0.836
	118.5		4.49-25	1.25-26		1.52-24		3.73-26	4.98-26	0.749
	122.5		8.44-25	2.35-26		1.52-24		3.73-26	6.08-26	0.613
	125.5		1.35-24	3.76-26		1.41-24		3.46-26	7.22-26	0.479
	128.5		2.18-24	6.07-26		1.18-24		2.89-26	8.36-26	0.353
	131.5		3.05-24	8.50-26		9.57-25		2.35-26	1.09-25	0.217
	134.5		3.81-24	1.06-25		6.70-25		1.64-26	1.22-25	0.134
	137.5		4.16-24	1.16-25		4.67-25		1.15-26	1.28-25	0.090
	141.5		4.18-24	1.16-25		2.73-25		6.70-27	1.23-25	0.055
	145.5		3.82-24	1.06-25		1.54-25		3.78-27	1.10-25	0.034
	149.5		3.18-24	8.86-26		8.58-26		2.10-27	9.07-26	0.023
	153.5		2.21-24	6.16-26		4.61-26		1.13-27	6.27-26	0.018
Water Gap -33/+2	106.5	8.00-25	3.08-23	2.93-26	7.61-28	3.16-25	1.36-23	2.28-25	5.30-27	6.06-27
	110.5		5.35-26	1.39-27		3.07-25		7.13-27	8.52-27	0.837
	114.5		9.44-26	2.45-27		3.63-25		8.43-27	1.09-26	0.775
	118.5		1.66-25	4.31-27		3.94-25		9.15-27	1.35-26	0.680
	122.5		2.86-25	7.43-27		3.95-25		9.18-27	1.66-26	0.553
	125.5		4.13-25	1.07-26		3.60-25		8.36-27	1.91-26	0.439
	128.5		5.93-25	1.54-26		3.13-25		7.27-27	2.27-26	0.321
	131.5		7.30-25	1.90-26		2.69-25		6.25-27	2.53-26	0.248
	134.5		8.89-25	2.31-26		2.11-25		4.90-27	2.80-26	0.175
	137.5		9.70-25	2.52-26		1.50-25		3.49-27	2.87-26	0.122
	141.5		9.92-25	2.58-26		9.82-26		2.28-27	2.81-26	0.081
	145.5		9.19-25	2.39-26		6.15-26		1.43-27	2.53-26	0.056
	149.5		7.76-25	2.02-26		3.68-26		8.55-28	2.11-26	0.041
	153.5		5.70-25	1.48-26		2.10-26		4.88-28	1.53-26	0.032

Table A.1. Continued

Location	Axial level (cm)	A R _{XY}	A R _{XZ}	B R _{XY}	B R _{XZ}	B R _{YZ}	A+B R _{XYZ}	B R _{XYZ} /R _{XYZ}	A+B R _{XYZ} /R _{XYZ}	Φ R _{XYZ}	
C. B., 0°	106.5	4.17-25	1.73-23	2.36-26	5.69-28	1.71-25	7.85-24	1.25-25	2.72-27	3.29-27	0.827
	110.5		4.31-26	1.04-27		1.65-25		3.59-27	4.63-27	0.775	3.04+7
	114.5		7.38-26	1.78-27		1.94-25	4.23-27	6.01-27	0.704		3.95+7
	118.5		1.20-25	2.89-27		2.08-25	4.53-27	7.42-27	0.611		4.87+7
	122.5		1.85-25	4.46-27		2.07-25	4.51-27	8.97-27	0.503		5.89+7
	125.5		2.54-25	6.12-27		1.88-25	4.10-27	1.02-26	0.401		6.70+7
	128.5		3.27-25	7.88-27		1.71-25	3.72-27	1.16-26	0.321		7.62+7
	131.5		3.85-25	9.28-27		1.50-25	3.27-27	1.26-26	0.261		8.27+7
	134.5		4.44-25	1.07-26		1.26-25	2.74-27	1.34-26	0.204		8.80+7
	137.5		4.88-25	1.18-26		9.46-26	2.06-27	1.39-26	0.149		9.13+7
	141.5		4.98-25	1.20-26		6.53-26	1.42-27	1.34-26	0.106		8.80+7
	145.5		4.68-25	1.13-26		4.39-26	9.56-28	1.23-26	0.078		8.08+7
	149.5		4.02-25	9.69-27		2.76-26	6.01-28	1.03-26	0.058		6.76+7
	153.5		2.97-25	7.16-27		1.62-26	3.53-28	7.51-27	0.047		4.93+7
C. B., 10°	106.5	3.85-25	1.73-23	2.36-26	5.25-28	1.61-25	7.85-24	1.25-25	2.56-27	3.09-27	0.830
	110.5		4.31-26	9.59-28		1.65-25	3.38-27	4.34-27		0.779	2.85+7
	114.5		7.38-26	1.64-27		1.94-25	3.98-27	5.62-27		0.708	3.69+7
	118.5		1.20-25	2.67-27		2.08-25	4.27-27	6.94-27		0.615	4.56+7
	122.5		1.85-25	4.12-27		2.07-25	4.25-27	8.37-27		0.508	5.50+7
	125.5		2.54-25	5.65-27		1.88-25	3.86-27	9.51-27		0.406	6.24+7
	128.5		3.27-25	7.28-27		1.71-25	3.51-27	1.08-26		0.325	7.09+7
	131.5		3.85-25	8.57-27		1.50-25	3.08-27	1.17-26		0.264	7.68+7
	134.5		4.44-25	9.88-27		1.26-25	2.58-27	1.25-26		0.207	8.21+7
	137.5		4.88-25	1.09-26		9.46-26	1.94-27	1.28-26		0.151	8.41+7
	141.5		4.98-25	1.11-26		6.53-26	1.34-27	1.24-26		0.108	8.14+7
	145.5		4.68-25	1.04-26		4.39-26	9.00-28	1.13-26		0.080	7.42+7
	149.5		4.02-25	8.95-27		2.76-26	5.66-28	9.52-27		0.059	6.25+7
	153.5		2.97-25	6.61-27		1.62-26	3.32-28	6.94-27		0.048	4.56+7

Table A.1. Continued

Location	Axial level (cm)	A R _{XY}	A R _{XZ}	A R _{XYZ}	B R _{XY}	B R _{XZ}	B R _{XYZ}	A+B R _{XYZ}	B R _{XYZ} /R _{XY}	A+B R _{XYZ} /R _{XZ}	Φ _{A+B} XYZ
C. B. 21°	106.5	3.91-25	2.04-23	2.40-26	4.60-28	1.78-25	9.21-24	1.53-25	2.96-27	3.42-27	0.865
	110.5	4.39-26	8.41-28			1.99-25	3.84-27	4.68-27	0.820	3.07+7	
	114.5	7.59-26	1.45-27			2.35-25	4.54-27	5.99-27	0.758	3.93+7	
	118.5	1.28-25	2.45-27			2.53-25	4.89-27	7.34-27	0.666	4.82+7	
	122.5	2.08-25	3.99-27			2.54-25	4.91-27	8.90-27	0.552	5.84+7	
	125.5	2.90-25	5.56-27			2.29-25	4.43-27	9.99-27	0.443	6.56+7	
	128.5	3.91-25	7.49-27			2.05-25	3.96-27	1.15-26	0.346	7.55+7	
	131.5	4.67-25	8.95-27			1.79-25	3.46-27	1.24-26	0.279	8.14+7	
	134.5	5.54-25	1.06-26			1.47-25	2.84-27	1.34-26	0.211	8.80+7	
	137.5	6.06-25	1.16-26			1.07-25	2.07-27	1.37-26	0.151	9.00+7	
	141.5	6.20-25	1.19-26			7.34-26	1.42-27	1.33-26	0.107	8.73+7	
	145.5	5.79-25	1.11-26			4.75-26	9.18-28	1.20-26	0.076	7.88+7	
	149.5	4.95-25	9.49-27			2.97-26	5.74-28	1.01-26	0.057	6.63+7	
	153.5	3.69-25	7.07-27			1.69-26	3.27-28	0.40-27	0.044	4.86+7	
C. B. 25°	106.5	3.85-25	1.73-23	2.63-26	3.77-28	1.61-25	7.85-24	1.83-25	2.90-27	3.28-27	0.885
	110.5	4.67-26	6.69-28			2.41-25	3.83-27	4.50-27	0.851	2.95+7	
	114.5	8.20-26	1.17-27			2.86-25	4.54-27	5.71-27	0.795	3.75+7	
	118.5	1.43-25	2.05-27			3.07-25	4.87-27	6.92-27	0.704	4.54+7	
	122.5	2.39-25	3.42-27			3.08-25	4.89-27	8.31-27	0.588	5.46+7	
	125.5	3.37-25	4.83-27			2.80-25	4.44-27	9.27-27	0.479	6.09+7	
	128.5	4.70-25	6.73-27			2.47-25	3.92-27	1.07-26	0.368	7.03+7	
	131.5	5.69-25	8.15-27			2.14-25	3.40-27	1.16-26	0.294	7.62+7	
	134.5	6.86-25	9.80-27			1.72-25	2.73-27	1.25-26	0.218	8.21+7	
	137.5	7.47-25	1.07-26			1.24-25	1.97-27	1.27-26	0.155	8.34+7	
	141.5	7.65-25	1.10-26			8.38-26	1.33-27	1.23-26	0.108	8.08+7	
	145.5	7.12-25	1.02-26			5.22-26	8.28-28	1.10-26	0.075	7.22+7	
	149.5	6.06-25	8.68-27			3.20-26	5.08-28	9.19-26	0.055	6.03+7	
	153.5	4.49-25	6.43-27			1.87-26	2.97-28	6.73-27	0.044	4.42+7	

Table A.1. Continued

Location	Axial level (cm)	$A_{R_{XY}}$	$A_{R_{XZ}}$	$A_{R_{YZ}}$	$B_{R_{XY}}$	B_{R_X}	$B_{R_{XZ}}$	$B_{R_{YZ}}$	$A+B_{R_{XYZ}}$	$B_{R_{XYZ}/B_{XYZ}}$	$A+B_{R_{XYZ}}$	$\phi_{R_{XYZ}}$
C, B, 28°	106.5	3.14-25	3.08-23	2.93-26	2.99-28	1.70-25	1.36-23	2.28-25	2.85-27	3.15-27	0.905	2.0747
	110.5			5.35-26	5.45-28			3.07-25	3.84-27	4.39-27	0.876	2.8847
	114.5			9.44-26	9.62-28			3.63-25	4.54-27	5.50-27	0.825	3.61+7
	118.5			1.66-25	1.69-27			3.94-25	4.93-27	6.62-27	0.745	4.35+7
	122.5			2.86-25	2.92-27			3.95-25	4.94-27	7.86-27	0.628	5.16+7
	125.5			4.13-25	4.21-27			3.60-25	4.50-27	8.71-27	0.517	5.72.7
	128.5			5.93-25	6.05-27			3.13-25	3.91-27	9.96-27	0.393	6.54+7
	131.5			7.30-25	7.44-27			2.69-25	3.36-27	1.08-26	0.311	7.09+7
	134.5			8.89-25	9.06-27			2.11-25	2.64-27	1.17-26	0.226	7.68+7
	137.5			9.70-25	9.89-27			1.50-25	1.88-27	1.18-26	0.160	7.75+7
	141.5			9.92-25	1.01-26			9.82-26	1.23-27	1.13-26	0.109	7.42+7
	145.5			9.19-25	9.37-27			6.15-26	7.69-28	1.01-26	0.076	6.63+7
	149.5			7.76-25	7.91-27			3.68-26	4.60-28	8.37-27	0.055	5.50+7
	153.5			5.70-25	5.81-27			2.10-26	2.63-28	6.07-27	0.043	3.99+7
C, B, 33°	106.5	2.78-25	5.56-23	4.02-26	2.01-28	1.70-25	2.40-23	4.01-25	2.84-27	3.04-27	0.934	2.00+7
	110.5			7.66-26	3.83-28			5.57-25	3.95-27	4.33-27	0.912	2.84+7
	114.5			1.41-25	7.05-28			6.66-25	4.72-27	5.43-27	0.870	3.57+7
	118.5			2.58-25	1.29-27			7.28-25	5.16-27	6.45-27	0.800	4.24+7
	122.5			4.65-25	2.33-27			7.27-25	5.15-27	7.48-27	0.689	4.91+7
	125.5			7.12-25	3.56-27			6.72-25	4.76-27	8.32-27	0.572	5.46+7
	128.5			1.07-24	5.35-27			5.70-25	4.04-27	9.39-27	0.430	6.17+7
	131.5			1.38-24	6.90-27			4.79-25	3.39-27	1.03-26	0.329	6.76+7
	134.5			1.70-24	8.50-27			3.54-25	2.51-27	1.10-26	0.228	7.22+7
	137.5			1.83-24	9.15-27			2.52-25	1.79-27	1.09-26	0.164	7.16+7
	141.5			1.89-24	9.45-27			1.56-25	1.11-27	1.06-26	0.105	6.96+7
	145.5			1.74-24	8.70-27			9.20-26	6.52-28	9.35-27	0.070	6.14+7
	149.5			1.45-24	7.25-27			5.24-26	3.71-28	7.62-27	0.049	5.00+7
	153.5			1.03-24	5.15-27			2.90-26	2.05-28	5.36-27	0.038	3.52+7

Table A.1. Continued

A-7

Location	Axial level	$A_{R_{XY}}$	A_{R_X}	$A_{R_{XYZ}}$	$B_{R_{XY}}$	B_{R_X}	$B_{R_{XYZ}}$	$B_{R_{XYZ}/R_{XYZ}}$	$A+B_{R_{XYZ}}$	$B_{R_{XYZ}/R_{XYZ}}$	$A+B_{R_{XYZ}}$
C, B, 40°	106.5	2.23-25	1.54-22	7.27-26	1.05-28	1.66-25	5.98-23	9.96-25	2.76-27	2.87-27	0.963
	110.5		1.43-25	2.07-28		1.42-24	3.94-27	4.15-27	0.950	2.73+7	
	114.5		2.72-25	3.94-28		1.74-24	4.83-27	5.22-27	0.925	3.43+7	
	118.5		5.17-25	7.49-28		1.93-24	5.36-27	6.11-27	0.877	4.01+7	
	122.5		9.87-25	1.43-27		1.93-24	5.36-27	6.79-27	0.789	4.46+7	
	125.5		1.61-24	2.33-27		1.80-24	5.00-27	7.33-27	0.682	4.81+7	
	128.5		2.71-24	3.92-27		1.49-24	4.14-27	8.06-27	0.514	5.29+7	
	131.5		4.17-24	6.04-27		1.19-24	3.30-27	9.34-27	0.353	6.13+7	
	134.5		5.17-24	7.49-27		8.09-25	2.25-27	9.76-27	0.231	6.40+7	
	137.5		5.60-24	8.11-27		5.54-25	1.54-27	9.65-27	0.160	6.36+7	
	141.5		5.59-24	8.09-27		3.17-25	8.80-28	8.97-27	0.098	5.89+7	
	145.5		5.09-24	7.37-27		1.79-25	4.97-28	7.87-27	0.063	5.17+7	
	149.5		4.23-24	6.13-27		9.95-26	2.76-28	6.41-27	0.043	4.21+7	
	153.5		2.98-24	4.32-27		5.36-26	1.49-28	4.47-27	0.033	2.96+7	
C, B, 45°#	106.5	2.19-25	2.73-23	8.31-26	6.67-29	1.82-25	2.64-22	3.65-27	3.72-27	0.982	2.46+7
	110.5		1.62-25	1.30-28		7.20-24	4.96-27	5.09-27	0.974	3.34+7	
	114.5		3.18-25	2.55-28		8.87-24	6.11-27	6.37-27	0.960	4.18+7	
	118.5		6.22-25	4.99-28		1.01-23	6.96-27	7.46-27	0.933	4.90+7	
	122.5		1.25-24	1.00-27		1.96-23	7.31-27	8.31-27	0.880	5.46+7	
	125.5		2.19-24	1.76-27		1.03-23	7.13-27	8.86-27	0.801	5.82+7	
	128.5		4.18-24	3.35-27		8.65-24	5.96-27	9.31-27	0.640	6.11+7	
	131.5		8.76-24	7.03-27		4.11-24	2.83-27	9.86-27	0.287	6.47+7	
	134.5		1.05-23	8.42-27		2.14-24	1.48-27	9.90-27	0.149	6.50+7	
	137.5		1.09-23	8.74-27		1.22-24	8.41-28	9.58-27	0.088	6.29+7	
	141.5		1.04-23	8.34-27		6.03-25	4.16-28	8.76-27	0.048	5.75+7	
	145.5		9.21-24	7.39-27		3.06-25	2.11-28	7.60-27	0.028	4.99+7	
	149.5		7.51-24	6.02-27		1.56-25	1.08-28	6.13-27	0.018	6.03+7	
	153.5		5.51-24	4.42-27		7.89-26	5.44-29	4.47-27	0.012	2.94+7	

Table A.1. Continued

Location	Axial level (cm)	A	A	B	B	B	B	B
		R _{XY}	R _{XZ}	R _{YZ}	R _{XY}	R _{XZ}	R _{YZ}	R _{XY}
C, B, 68°#	106.5	4.56-25	2.51-23	2.84-26	5.16-28	4.41-25	2.43-23	4.18-25
	110.5		5.10-26	9.27-28		5.79-25	1.05-26	1.16-26
	114.5		8.98-26	1.63-27		6.88-25	1.25-26	1.41-26
	118.5		1.55-25	2.82-27		7.50-25	1.36-26	1.64-26
	122.5		2.56-25	4.65-27		7.42-25	1.35-26	1.82-26
	125.5		3.60-25	6.54-27		6.86-25	1.24-26	1.82-26
	128.5		4.95-25	8.99-27		5.77-25	1.05-26	1.89-26
	131.5		5.92-25	1.08-26		4.83-25	8.77-27	1.95-26
	134.5		7.05-25	1.28-26		3.51-25	6.37-27	1.96-26
	137.5		7.64-25	1.39-26		2.49-25	4.52-27	1.92-26
	141.5		7.75-25	1.41-26		1.51-25	2.74-27	1.84-26
	145.5		7.14-25	1.30-26		8.71-26	1.58-27	1.68-26
	149.5		6.04-25	1.10-26		4.92-26	8.93-28	1.46-26
	153.5		4.45-25	8.08-27		2.72-26	4.94-28	1.19-26
C, B, 89°#	106.5	4.97-25	2.07-23	2.79-26	6.70-28	4.85-25	2.00-23	3.32-25
	110.5		5.11-26	1.23-27		4.59-25	1.11-26	1.23-26
	114.5		8.83-26	2.12-27		5.40-25	1.31-26	1.52-26
	118.5		1.45-25	3.48-27		5.86-25	1.42-26	1.77-26
	122.5		2.24-25	5.38-27		5.81-25	1.41-26	1.95-26
	125.5		3.11-25	7.47-27		5.31-25	1.29-26	2.04-26
	128.5		4.03-25	9.68-27		4.60-25	1.12-26	2.09-26
	131.5		4.73-25	1.14-26		3.92-25	9.51-27	2.09-26
	134.5		5.47-25	1.31-26		3.03-25	7.35-27	2.05-26
	137.5		5.98-25	1.44-26		2.18-25	5.29-27	1.97-26
	141.5		6.04-25	1.45-26		1.41-25	3.42-27	1.79-26
	145.5		5.61-25	1.35-26		8.57-26	2.08-27	1.56-26
	149.5		4.79-25	1.15-26		4.93-26	1.20-27	1.27-26
	153.5		3.50-25	8.40-27		2.67-26	6.47-28	9.05-27

*Reaction rates in units of reactions/s•nucleus per 639 fissions/s•quadrant appearing in the third column from the right have been multiplied by the factor (8.845x10⁹/1.347x10⁻²⁴) to convert to fission equivalent fluxes at 100% power.

† Read as 3.26x10⁻²⁴.

#Calculations based on orientation of X and Y axes rotated 90° to that in Fig. 1.

BIBLIOGRAPHIC DATA SHEET

(See instructions on the reverse)

1. REPORT NUMBER
(Assigned by NRC. Add Vol., Supp., Rev.,
and Addendum Numbers, if any.)

NUREG/CR-5338
ORNL/TM-11106

2. TITLE AND SUBTITLE

Analysis of the VENUS-3 Experiments

3. DATE REPORT PUBLISHED

MONTH	YEAR
August	1989

4. FIN OR GRANT NUMBER
B0415

5. AUTHOR(S)

R. E. Maerker

6. TYPE OF REPORT

Technical

7. PERIOD COVERED (Inclusive Dates)

8. PERFORMING ORGANIZATION - NAME AND ADDRESS (If NRC, provide Division, Office or Region, U.S. Nuclear Regulatory Commission, and mailing address; If contractor, provide name and mailing address.)

Oak Ridge National Laboratory
P. O. Box 2008
Oak Ridge, Tennessee 37831

9. SPONSORING ORGANIZATION - NAME AND ADDRESS (If NRC, type "Same as above"; If contractor, provide NRC Division, Office or Region, U.S. Nuclear Regulatory Commission, and mailing address.)

Division of Engineering
Office of Nuclear Regulatory Research
U. S. Nuclear Regulatory Commission
Washington, DC 20555

10. SUPPLEMENTARY NOTES

11. ABSTRACT (200 words or less)

The results of applying a hybrid superposition-synthesis calculational method to a mockup of a three-dimensional geometry involving a partial length shield assembly (PLSA) at the VENUS-3 facility in Mol, Belgium, are described. Comparisons of transport calculations using the method and many measurements involving nickel, indium, and aluminum dosimeters indicate agreement generally to within five percent if effects of inaccuracies in the dosimeter cross sections are minimized and proper orientation of the coordinate system used in the synthesis procedure is observed. These conclusions bode well for the success of this method in solving neutron transport problems involving the use of PLSSAs in light water reactors to reduce core leakage in pressurized thermal shock programs.

A second report describing the experimental details of the measurements will serve as companion documentation to this one and will be furnished by the Studiecentrum voor Kernenergie/Centre d'Etude de l'Energie Nucleaire, Mol, Belgium.

12. KEY WORDS/DESCRIPTORS (List words or phrases that will assist researchers in locating the report.)

transport calculations
neutron transport
VENUS-3

13. AVAILABILITY STATEMENT

Unlimited

14. SECURITY CLASSIFICATION

(This Page)

Unclassified

(This Report)

Unclassified

15. NUMBER OF PAGES

16. PRICE

UNITED STATES
NUCLEAR REGULATORY COMMISSION
WASHINGTON, D.C. 20555

SPECIAL FOURTH-CLASS RATE
POSTAGE & FEES PAID
USNRC
PERMIT No. G-67

OFFICIAL BUSINESS
PENALTY FOR PRIVATE USE, \$300

120555139531 1 1AN1RL
US NRC-QADM
DIV FOIA & PUBLICATIONS SVCS
TPS PDR-NUREG
P-209
WASHINGTON

DC 20555